# An Investigation of Spectral Broadening by Nonlinear Optical Effects in Photonic Crystal Fibers

By
MacAulay James Harvey

A Thesis Submitted to

Saint Mary's University, Halifax, Nova Scotia
in Partial Fulfillment of the Requirements for the Degree of
Bachelor of Science with Honours in Physics

May 2021, Halifax, Nova Scotia

© MacAulay Harvey, 2021

# An Investigation of Spectral Broadening by Nonlinear Optical Effects in Photonic Crystal Fibers

*by*

MacAulay James Harvey

## Abstract

When a pulse of light with sufficient power moves through optical fiber its spectrum broadens as a result of nonlinear optical effects such as self-phase modulation, self-steepening, and stimulated Raman scattering. This spectral broadening is of great interest because it can be used to construct a simple wavelength tunable laser source for nonlinear optical microscopy. Nonlinear optical microscopy is a form of microscopy which utilizes nonlinear optical effects within a sample as a contrast mechanism. This includes effects such as second-harmonic generation, third-harmonic generation, and coherent anti-Stokes Raman Scattering. These forms of microscopy have been shown to have applications in medical imaging, including as possible tools for accurately diagnosing certain cancers.

This thesis explores the use of nonlinear optical effects to broaden the spectrum of ultrashort pulses of light. This is done through experimental work in which the effects of pulse energy, pulse duration, and fiber length on spectral broadening are explored. Numerical simulations of the equations of optical pulse propagation are also used in order to evaluate which effects dominate the spectrum of an ultrashort optical pulse, and to investigate the effect of pulse shape on the resulting spectrum. These results will be helpful in evaluating the usefulness of spectral broadening in optical fiber in the construction of a wavelength tunable laser source for nonlinear optical microscopy.

Date: 5 May 2021

# Contents

# List of Abbreviations and Acronyms

SRS . . . . . Stimulated Raman scattering

CARS . . . . . Coherent anti-Stokes Raman Scattering

GVD . . . . . Group velocity dispersion

SPM . . . . . Self-phase modulation

# List of Figures

# List of Tables

# **Chapter 1:** Introduction

## 1.1 Background and Motivation

The field of fiber optics has its roots in the mid-19$^{th}$ century when Swiss physicist Jean-Daniel Colladon demonstrated that a beam of light could be confined to a jet of water through total internal reflection. Over the next hundred years light guiding by total internal reflection was used for various applications, for example bent glass rods where often used to guide light into body cavities during surgery. Modern optical fiber with a dielectric cladding surrounding a core was first produced in the 1950s, the addition of a cladding enabled the production of very thin, flexible fibers which are now commonplace. Slowly over the next thirty years low loss optical fibers suitable for telecommunications applications began to be mass produced, with the most common fibers having a core and cladding made from glass where the cladding has a slightly lower refractive index than the core [1].

The widespread availability of low loss optical fibers, with losses of 0.2 dB/km or less [2], led to the ability to produce various nonlinear optical effects within the fiber including four-wave mixing, stimulated Brillouin scattering, stimulated Raman scattering (SRS), and self-phase modulation [3]–[6]. The development of commercial pulsed lasers, which are currently able to produce optical pulses on the scale of femtoseconds, enable the production of optical pulses with high peak powers while keeping average power low. These high peak powers allow nonlinear effects to have a great effect on the spectrum of an optical pulse as it moves through optical fiber. These nonlinear effects are of great interest since they can be used to modulate the

spectrum of a pulse of light that is propagating through a fiber, which enables the construction of a simple wavelength tunable laser source. Although several techniques currently exist for the production of a wavelength tunable laser source, for example the optical parametric oscillator, these techniques often require very complicated and expensive set ups which require frequent maintenance. Through fiber-based wavelength tuning laser sources can be produced which are much cheaper, and simpler to construct than currently available alternatives. A potential application of this is in the construction of a wavelength tunable laser source for nonlinear optical microscopy.

Nonlinear optical microscopy includes various microscopy techniques which utilize nonlinear optical effects within the sample being imaged as a contrast mechanism, this includes three wave mixing techniques such as second harmonic generation and sum-frequency generation, as well as four-wave mixing techniques such as third harmonic generation, and coherent anti-Stokes Raman Scattering (CARS) microscopy. Pulsed laser sources are needed for nonlinear optical microscopy since nonlinear effects require very high peak power, but average power must be kept low to avoid damaging biological samples. These microscopy techniques are advantageous since they can allow a sample to be visualized without the need for dyes and can reduce the effect of photobleaching compared to fluorescence microscopy techniques. The addition of a wavelength tunable laser source would allow for a greater range of samples that could be imaged using these techniques and would enable investigations into the wavelength dependence of nonlinear optical phenomena. This has some very exciting applications particularly in the field of medical imaging since several forms of nonlinear optical microscopy have been shown to be effective tools in the diagnosis of certain forms of cancer, as well as other diseases [7], [8]. The investigation of the nonlinear optical properties of optical fiber has also

been shown to have applications in areas such as telecommunications, fast analogue to digital conversion, and slow light [9], [10].

## 1.2 Methods for Spectral Broadening

Various methods have been used to alter spectrum laser pulses using optical fiber. The simplest of these methods relies primarily on self-phase modulation, the dominant nonlinear optical effect in optical fiber which occurs as a result of the optical Kerr effect. Self-phase modulation has the effect of splitting a pulse spectrum with an initially Gaussian profile into two dominant spectral lobes, one of which is shifted to the shorter wavelengths, the other to the higher wavelengths as shown in Fig 1.1. This technique has been shown to be very effective at producing a broad spectrum laser source, previous results have shown that spectral broadening from self-phase modulation can be used to broaden an initially narrow pulse spectrum centered at 1030 nm such that the spectrum ranges from 825 to 1210 nm [11]. By using spectral filters to isolate either of the dominant spectral lobes self-phase modulation has been used to produce optical pulses with center wavelengths shifted nearly 200 nm with 20 nJ pulse energies and less than 90 fs pulse durations (from 190 fs initial duration), this was shown to be an effective laser source for use in nonlinear optical microscopy applications [12]. For ultrafast laser pulses on the order of 5 ps or less, other dispersive and nonlinear optical effects start to affect how the fiber changes the pulse spectrum. It will be necessary to consider these other effects since laser sources for nonlinear optical microscopy typically have pulse durations ranging from 50 to 500 fs. These higher order effects lead to much more complicated output spectra which usually require numerical simulations to be accurately predicted [11].

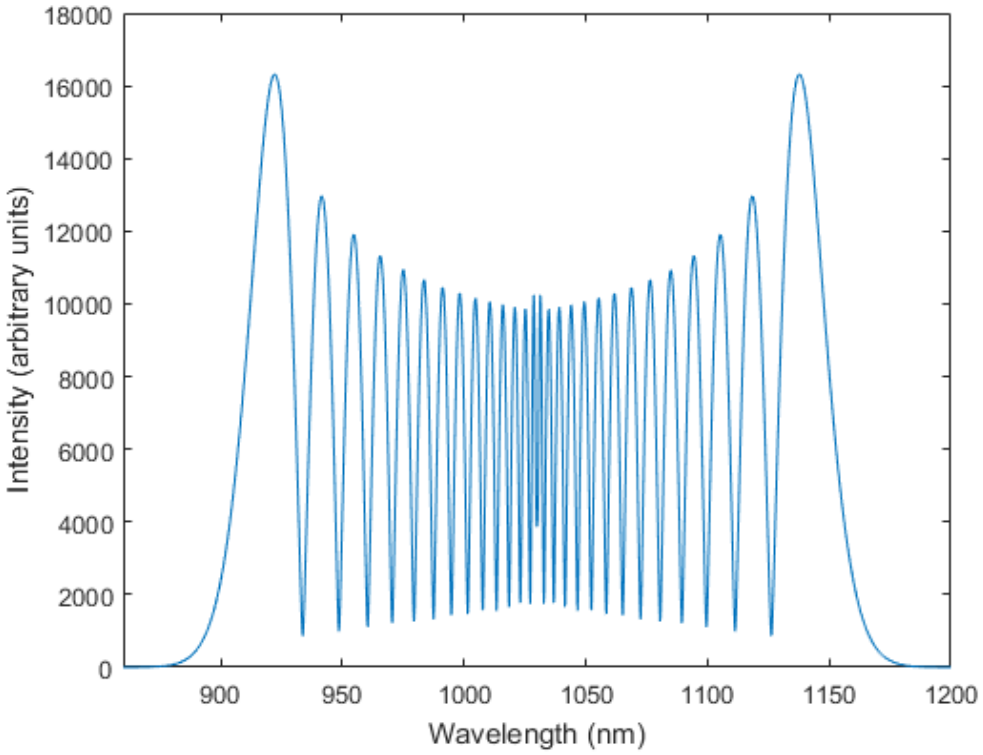


Fig 1.1: Simulation showing a spectrum which has been broadened by self-phase modulation.

Another commonly used technique for modifying the wavelength spectrum of a laser pulse is known as supercontinuum generation. Supercontinuum generation utilizes a large variety of optical effects acting together on the pulse in order to create a very broad pulse spectrum an example of which is shown in Fig 1.2. Experimental work has shown that a supercontinuum from 1100 to 1700 nm can be generated in silica photonic crystal fibers using pulse with a peak power of 1.38 kW, initial center wavelength of 1300 nm, and duration of 600 fs [13]. Numerical simulations are also commonly used to give a more detailed picture of how supercontinuum form within optical fiber [13], [14]. Supercontinuum generation has been shown to be useful in microscopy applications such as optical coherence tomography and CARS microscopy [13], [14], and is generally used in applications where a very broad spectrum is required. However,

due to the broadness of the spectra generated, the power density of the spectrum is greatly reduced. This means that supercontinuum generation is not an efficient method of laser wavelength tuning if only a small range of wavelengths is desired.

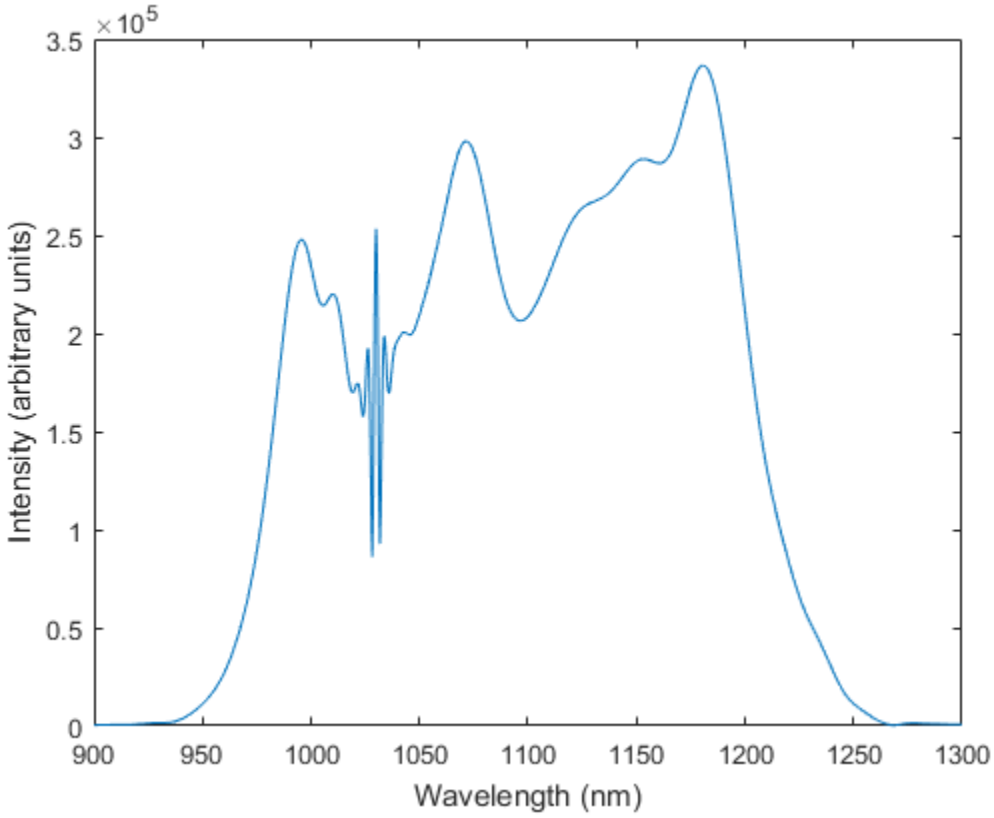


Fig 1.2: Simulation showing a typical supercontinuum spectrum.

A major disadvantage of both pure self-phase modulation and supercontinuum generation for many applications is that they both produce very broad spectra. This makes these methods inefficient for wavelength tuning if an output with a similar spectral power density to the input and a shifted center wavelength is desired. In this case a better way of tuning laser wavelength utilizes an effect known as soliton self-frequency shift. This effect uses a soliton, a pulse of light

which is able to propagate with no change to its temporal profile or spectrum, which is being influenced by SRS. This results in the pulse spectrum being continuously redshifted as it propagates through an optical fiber [15] such as that shown in Fig 1.3. This technique has been used extensively for wavelength tuning in nonlinear optical microscopy applications, and has can used to shift the center wavelength of a pulse by up to 200 nm with pulse energies of approximately 140 nJ [16], however higher pulse energies have been shown to yield a shift in center wavelength of nearly 1000 nm [17]. Soliton self-frequency shift has been applied to a variety of optical microscopy techniques such as two-photon excited fluorescence imaging, second harmonic generation, and third harmonic generation microscopy [16], [17]. Numerical simulations are often used to predict the amount of wavelength shift which can be achieved for a given fiber, and to study the stability of optical solitons [18]. Soliton self-frequency shift is advantageous because ideally the pulse spectrum is not broadened and has its center wavelength shifted, meaning that wavelength tuning can be done more efficiently than by other methods. However, in order to take advantage of soliton self-frequency shift the optical effects acting on a pulse as it propagates through optical fiber must balance in such a way that SRS is the dominant effect on the pulse. Otherwise, other optical effects would be dominant, and the resulting spectrum would look more like a self-phase modulation broadened, or a supercontinuum spectrum.

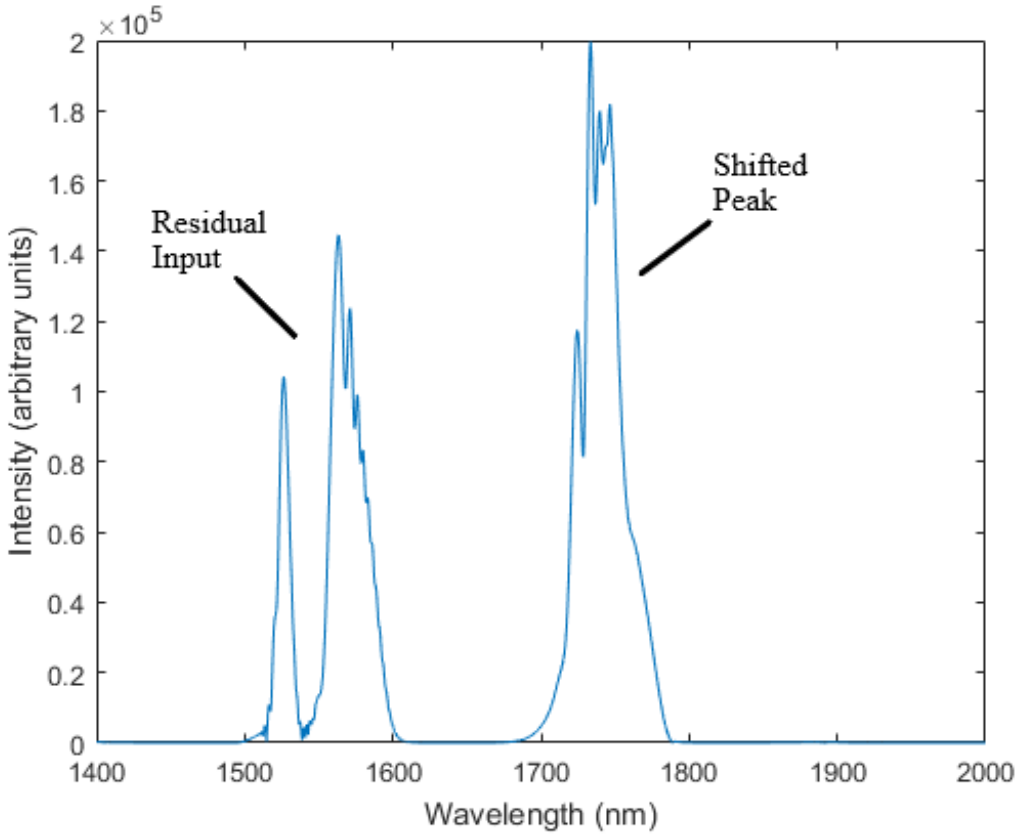


Fig 1.3: Simulated spectrum showing the effect of soliton self-frequency shift.

## 1.3 Objectives

The goal of this thesis is to investigate how the spectrum of a 1030 nm laser with 245 fs pulse duration is changed by nonlinear optical effects in a photonic crystal optical fiber. An emphasis is placed on how these effects can be used for laser wavelength tuning for applications in nonlinear optical microscopy. This is accomplished through experimental work in which commercially available photonic crystal fibers are free space coupled to the laser. The pulse energy and duration of the laser are then varied, and the spectrum of the output pulse is

measured. This allows for the gathering of data on how to optimize the various laser and fiber parameters in order to achieve efficient laser wavelength tuning.

This experimental work is augmented by the use of simulations in which the equations governing pulse propagation in optical fiber are solved numerically. These simulations give more detailed knowledge on how the various effects within optical fiber change the spectrum of a laser pulse as it propagates. The effects of laser pulse shape, and duration can also be studied more easily through the use of simulations.

# **Chapter 2 :** Theory of Light-Matter Interactions in Optical Fibers

As an optical pulse moves through optical fiber it is acted on by a large variety of optical effects. This chapter will provide a brief overview of the dominant optical effects for optical pulses with durations of less than a few picoseconds. An equation which can be used to model the propagation of pulses in optical fiber will also be discussed.

## 2.1 Introduction to light-matter interactions

### 2.1.1 Group Velocity Dispersion

The simplest optical effect within optical fiber is group velocity dispersion (GVD). To understand how this effect comes about consider the formula for the speed of light in a medium.

$$v = \frac{c}{n} \tag{2.1}$$

Where $v$ is the phase velocity of light in the medium, $c$ is the speed of light in a vacuum, and $n$ is the refractive index of the material. Typically, the refractive index of a material will be dependent on the wavelength of the incident light, as a result of this the different spectral components of an optical pulse will propagate at different speeds through a medium. This can result in pulses becoming significantly broadened in time as they propagate as shown in Fig 2.1. This effect is known as group velocity dispersion.

To get an idea of how GVD effects the propagation of a pulse of light we expand the propagation constant, which represents the change in phase per unit length of a pulse traveling in a medium, of the pulse in a power series about the pulse's center frequency $\omega_0$ [2].

$$\beta(\omega) = n(\omega)\frac{\omega}{c} = \beta_0 + \beta_1(\omega - \omega_0) + \frac{1}{2}\beta_2(\omega - \omega_0)^2 + \frac{1}{6}\beta_3(\omega - \omega_0)^3 \quad (2.2)$$

Where $$\beta_n = \left(\frac{d^n\beta}{d\omega^n}\right)_{\omega=\omega_0},$$

and $\omega$ represents frequencies within the spectral width of the pulse, and $\beta$ is the propagation constant which is assumed to be frequency dependent. Here $\beta_1$ is related to the group velocity $(v_g)$ of the pulse $\beta_1 = \frac{1}{v_g}$, $\beta_2$ represents the dispersion of group velocity and is therefore known as the GVD parameter. Here it is assumed that the pulses have a small enough spectral width that $(\omega - \omega_0)^2 \gg (\omega - \omega_0)^3$ and therefore terms of third order and above are neglected (the effects of third order terms are discussed in section 2.2.1).

For visible light the refractive index of a material typically decreases with increasing wavelength meaning that $\beta_2$ is positive this is referred to as normal dispersion. If the refractive index increases with increasing wavelength then $\beta_2$ is negative, this is referred to as anomalous dispersion. Fused silica, a very common material in optical fibers, exhibits normal dispersion for wavelengths less than 1270 nm and anomalous dispersion at wavelengths greater than 1270 nm where 1270 nm is the zero dispersion wavelength of fused silica [2].

The effect of GVD is especially noticeable for ultrashort optical pulses with durations of several picoseconds or less. This is due to the time-bandwidth product, which arises as a result of the uncertainty principle. The time bandwidth product states that the product between the pulse duration and spectral bandwidth must be greater than or equal to a constant (where the value of the constant is determined by the pulse shape). A pulse which has the minimum spectral width

for its duration is said to be transform limited. The consequence of the time-bandwidth product is that as the pulse duration is decreased its spectral width must increase. This results in GVD having a greater effect on shorter optical pulses.

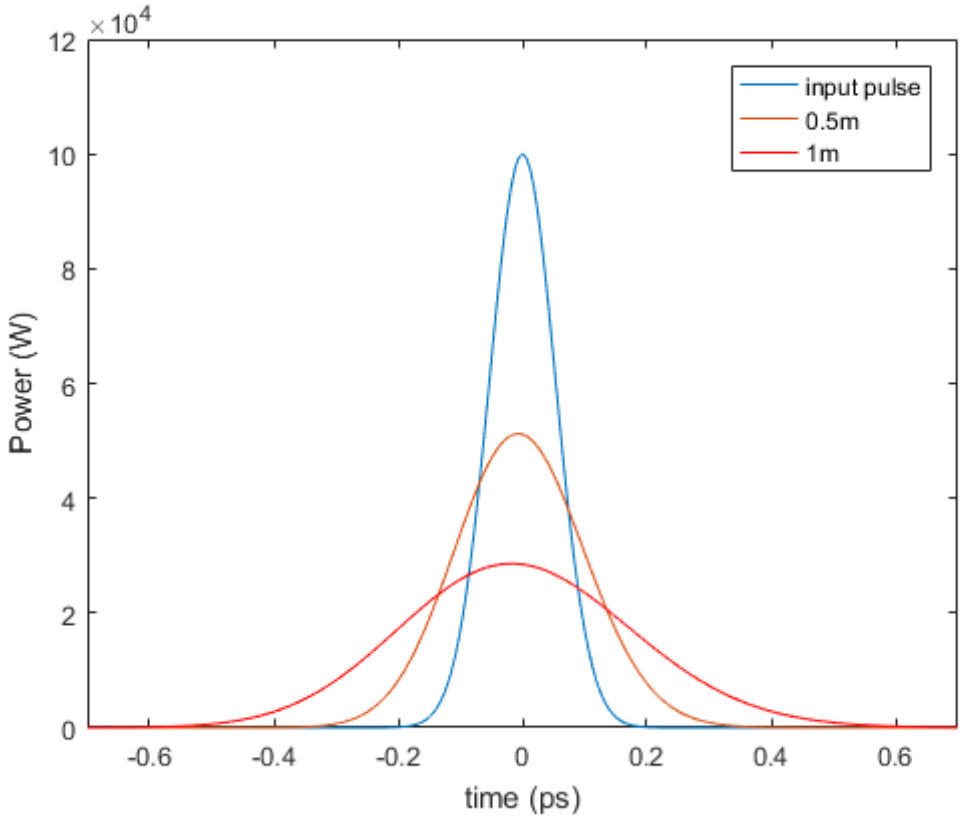


Fig 2.1: Simulations showing the effect of GVD on a pulse at three fiber lengths.

## 2.1.2 Self-Phase Modulation

While GVD is the dominant time domain effect on a pulse propagating in optical fiber the dominant frequency domain effect is known as self-phase modulation (SPM). SPM is a nonlinear effect which comes about as a result of the optical Kerr effect, an effect in which the refractive index of a material changes with an applied electric field through the following relation [19],

$$n = n_0 + n_2 I \tag{2.3}$$

where $I$ is the optical intensity given by $I(t) = 2n_0\epsilon_0 c|U(z,t)|^2$ and $n_2$ is known as the nonlinear refractive index and is used to quantify the change in refractive index $n_0$ induced by an applied electric field. The nonlinear refractive index arises as a result of the third order electronic susceptibility of the material. Typically, the value of $n_2$ is much smaller than that of $n_0$.

This change in the refractive index of the material results in a change in the phase of an optical pulse. The magnitude of this phase change is given be the following equation

$$\phi(t) = -n_2 I(t)\omega_0 L/c \tag{2.4}$$

where $L$ is the length of the nonlinear medium that the pulse moves through. This phase change results in a change to the instantaneous frequency.

$$\omega(t) = \omega_0 + \frac{d}{dt}(\phi(t)) \tag{2.5}$$

This results in a change in an initially Gaussian pulse spectrum with the pulse splitting into two dominant spectral lobes, one of which becomes redshifted, and the other blue shifted in a symmetric manner as shown in Fig 2.2.

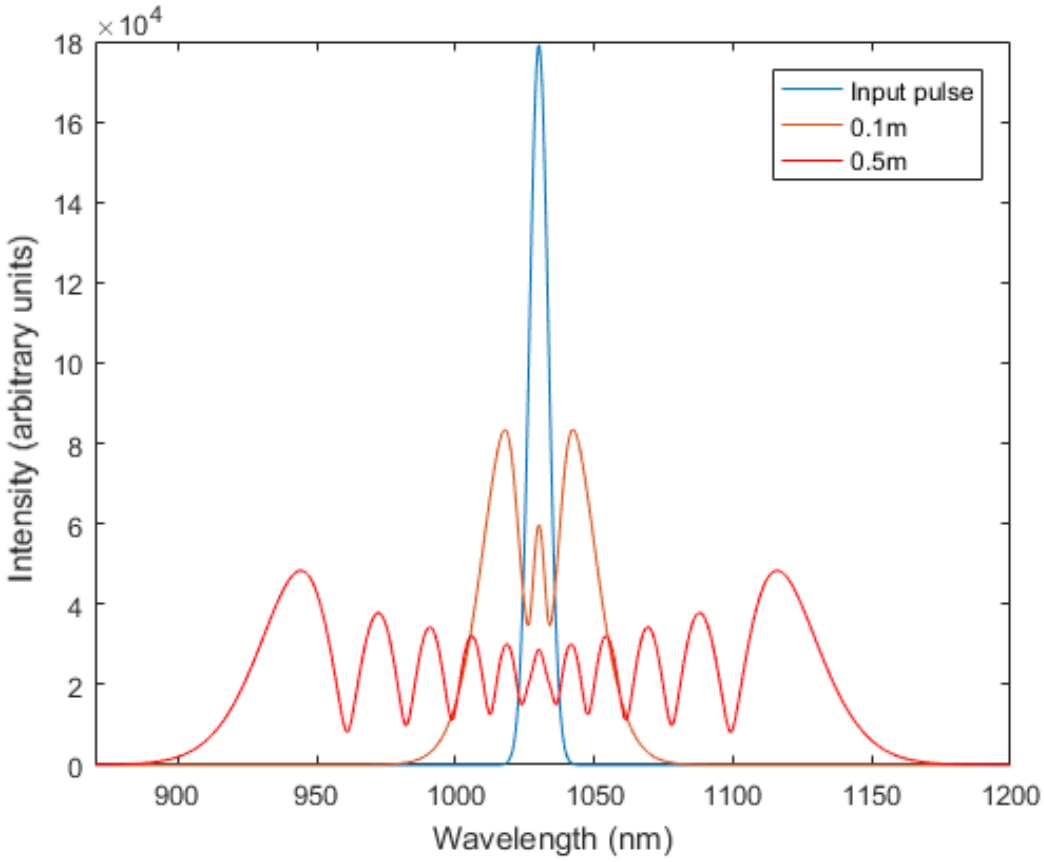


Fig 2.2: Simulations showing the effect of SPM (neglecting GVD) on a pulse over three lengths of fiber.

## 2.1.3 The Nonlinear Schrodinger Equation

By considering how the effects of GVD and SPM simultaneously effect the electric field envelope of an optical pulse the following equation can be derived,

$$\frac{\partial U}{\partial z} = -\frac{i\beta_2}{2}\frac{\partial^2 U}{\partial t^2} + i\gamma|U|^2U \tag{2.6}$$

where $U$ is the electric field envelope of the pulse, $\gamma$ is known as the nonlinearity of the fiber and is given by $\gamma = \frac{2\pi n_2}{\lambda A_{eff}}$ and $A_{eff}$ is the effective mode area of the fiber.

This equation is known as the nonlinear Schrodinger equation. This equation is often written such that $P = |U|^2$ where $P$ is power, the equation can then be expressed in a dimensionless form [18].

$$-i\frac{\partial U}{\partial z} = \frac{1}{2}\frac{\partial^2 U}{\partial t^2} + |U|^2 U \tag{2.7}$$

In the dimensionless form time, distance, and power are expressed in the soliton units defined below

$$t_c = \frac{\tau}{1.763} \quad z_c = \frac{{t_c}^2}{|\beta_2|} \quad P_c = \frac{\gamma}{z_c} \tag{2.8}$$

where $\tau$ is pulse duration at full width half maximum (FWHM).

When expressed in this form equation 2.7 has the particular solution

$$U(z,t) = \text{sech}\,(t)e^{\frac{iz}{2}} \tag{2.9}$$

This solution is interesting since its temporal profile does not change as the pulse propagates along $z$ as shown in Fig 2.3. Physically this means that the effects of GVD and SPM must cancel such that the pulse is able to propagate undisturbed. This is known as the fundamental soliton, and solutions of this form have been shown to have applications in telecommunications, and under the influence of higher order nonlinear effects can lead to soliton self-frequency shift (the effect which leads to self-frequency shift will be covered in section 2.2.2). The nonlinear Schrodinger equation also has solutions known as higher order solitons. These solutions exist for higher pulse powers than the fundamental soliton, and result in the pulse spectrum changing in a symmetric manner but periodically returning to its original shape [2].

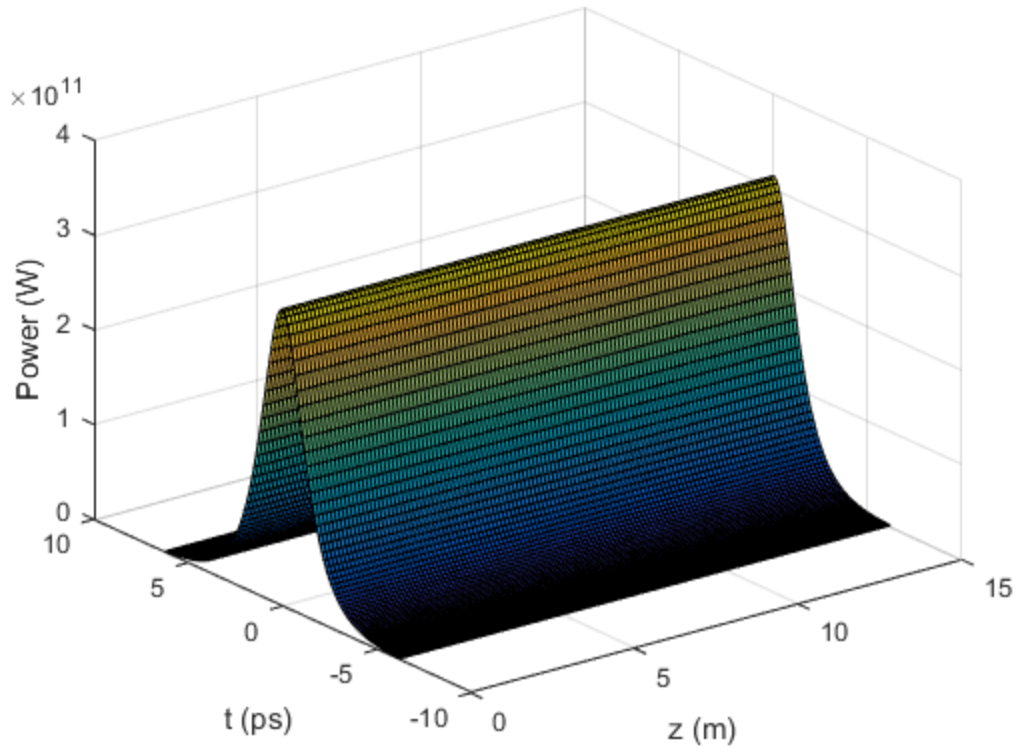


Fig 2.3: The power profile of the fundamental soliton as it propagates through optical fiber. Note that the effects of GVD and SPM balance allowing the pulse to move undisturbed through the fiber.

## 2.2 Higher Order Optical Effects

The previous section provided a brief overview of the dominant effects on a pulse of light as it propagates in optical fiber. Generally, the nonlinear Schrodinger equation presented in equation 2.7 provides a good approximation of the behaviour of pulses that are longer than a few picoseconds. However, for pulses with a duration on the order of picoseconds or less there are

several other optical effects including higher order dispersion, SRS, and self steepening, which should be considered in order to accurately predict how pulses of light propagate in optical fiber.

### 2.2.1 Higher Order Dispersion

When the power series representation of the propagation constant was considered in equation 2.2 only terms up to $\beta_2$ which represents group velocity dispersion were considered. This approximation is justified for longer pulse durations since these pulses have shorter spectral widths as a result of the time-bandwidth product. However, when pulses become very short their spectral width becomes sufficiently large that we can no longer say that $(\omega - \omega_0)^2 \gg (\omega - \omega_0)^3$ since there is now a greater difference between the different spectral components of the pulse. Because of this for ultrashort pulses of less than 5ps typically the effect of third order dispersion is considered in addition to GVD and the equation describing how an optical pulse is changed due to dispersive effects becomes:

$$\frac{\partial U}{\partial z} = -\frac{i\beta_2}{2}\frac{\partial^2 U}{\partial t^2} + \frac{\beta_3}{6}\frac{\partial^3 U}{\partial t^3} \tag{2.10}$$

where $\beta_3$ is known as the third order dispersion parameter. Fig 2.4 shows the effect of third order dispersion on an optical pulse with an initially Gaussian temporal profile.

It is important to note that many materials have a zero-dispersion wavelength at which the value of $\beta_2$ approaches zero. This can result in third order dispersion becoming the dominant dispersive effect, which might lead to instability in the temporal behaviour of the pulse.

In some applications, such as supercontinuum generation, where extremely broad spectra are produced it may also be necessary to consider dispersive terms of fourth order and above.

However, these higher order dispersive effects are usually found to be negligible [20], and will not be considered here.

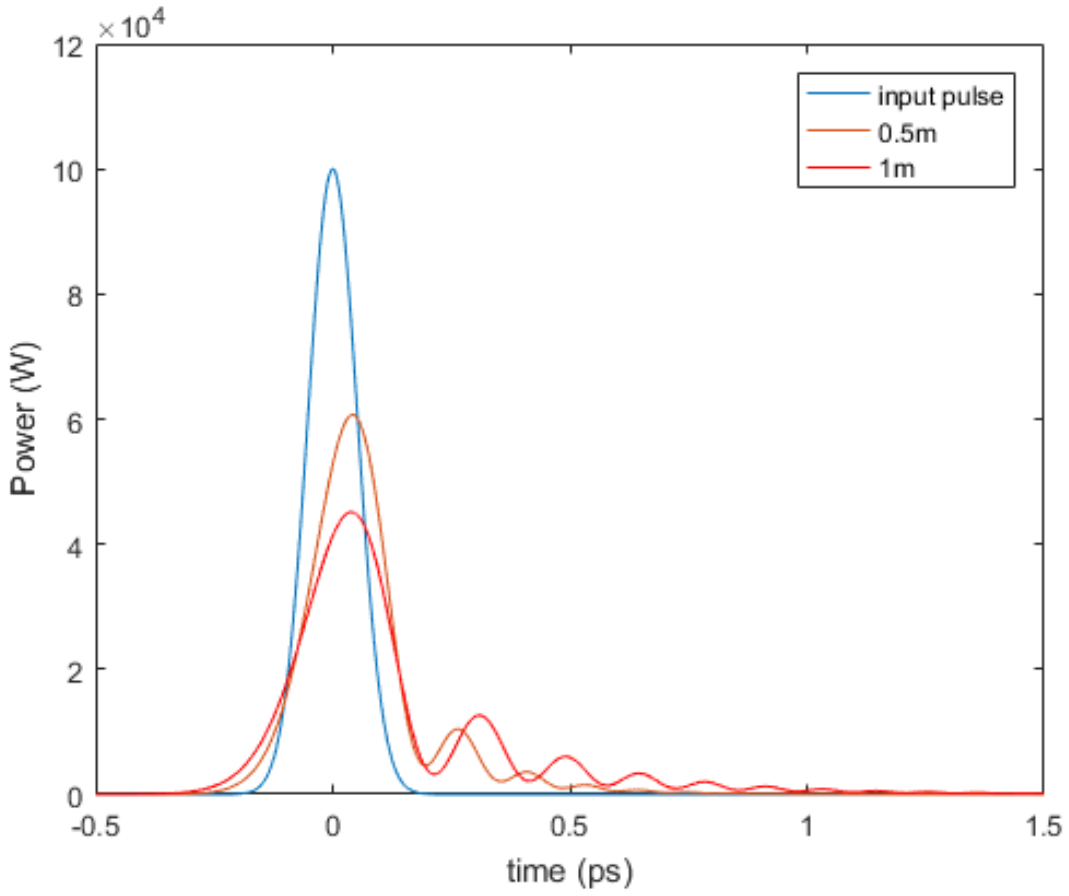


Fig 2.4: Simulation showing the effect of GVD and third order dispersion on a pulse over different lengths of fiber.

## 2.2.2 Stimulated Raman Scattering

As a pulse with high peak power propagates through optical fiber the molecules that make up the fiber can gain vibrational energy by inelastically scattering photons. This is known as spontaneous Raman scattering, and it has the effect of shifting the wavelength of the incident

photon from its original wavelength (known as the pump wavelength) to a higher wavelength (know as the Stokes wavelength). Spontaneous Raman scattering is a very inefficient process, and usually results in only a small fraction (typically 1 in $10^6$) of pump power being transferred to the Stokes wavelength [2]. However, the small number of Stokes photons resulting from spontaneous Raman scattering can stimulate further Raman scattering. In stimulated Raman scattering (SRS) a pump photon and a Stokes photon are both incident on a molecule at the same time. The pump photon is then scattered by the molecule and the presence of the Stokes photon results in the production of a further Stokes photon through stimulated emission. SRS is much more efficient than spontaneous Raman scattering and can result in 10% or more of incident photons being converted to the redshifted Stokes wavelength [19], these Stokes photon will then go on to stimulate further Raman scattering. This means that, if SRS is the sole effect acting on an optical pulse, longer lengths of optical fiber will result in a greater percentage of the input pulse photons being converted to the redshifted stokes wavelength. Electron energy level diagrams for spontaneous and stimulated Raman scattering are shown in Fig 2.5.

In addition to the red shifting which was considered here (known as stimulated Stokes Raman) it is also possible for SRS to result in a blue shift (known as stimulated anti-Stokes-Raman), however this is rarely seen in optical fiber due to phase-matching conditions which must be satisfied [2].

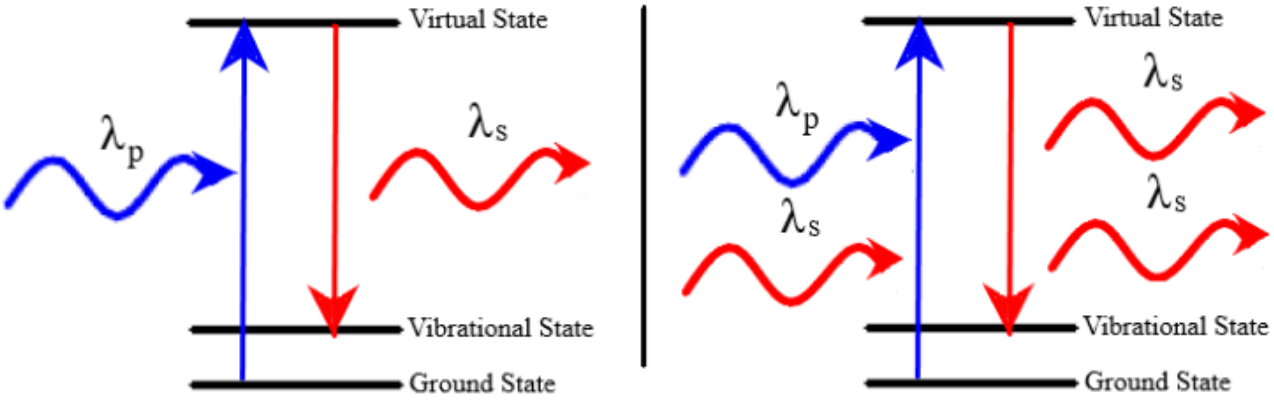


Fig 2.5: Electron energy level diagrams for spontaneous (left) and stimulated (right) Raman scattering. Here $\lambda_p$is the pump wavelength and $\lambda_S$ is the Stokes wavelength.

SRS is the main effect responsible for soliton self-frequency shift. Since in the case of a soliton pulse GVD and SPM effectively cancel each other out SRS can become the dominant optical effect. This results in the soliton becoming continuously redshifted as it propagates through the fiber. The effect of SRS on the spectrum of an optical pulse, where SPM and GVD are also considered, can be seen in Fig 2.6.

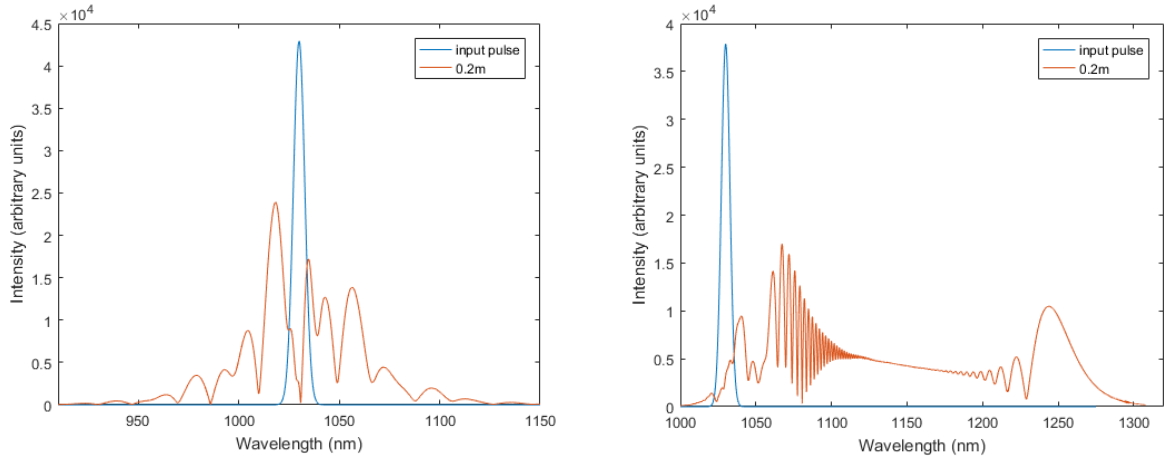


Fig 2.6: Simulations showing effects of GVD and SPM acting on a pulse (left) and GVD, SPM and SRS (right).

## 2.2.3 Self-Steepening

The group velocity of an optical pulse moving through optical fiber is typically dependent on the intensity of the pulse as a result of the intensity dependence of the refractive index shown in equation 2.3. As a result of this the center of a pulse will travel at a different speed than the two wings. This causes the temporal profile of the pulse to take on an increasingly asymmetric shape as it moves through the fiber, with one edge of the pulse appearing much steeper than the other. If self-steepening is allowed to be the dominant effect on an optical pulse it can lead to extremely short pulse durations, which can result in the formation of an optical shock wave [21]. Self-steepening acting in conjunction with SPM is known to cause the pulse's spectrum to broaden asymmetrically, rather that the purely symmetric broadening generated by SPM alone [2]. The effect of self steepening on the temporal profile and spectrum of an optical pulse is shown in Fig 2.7.

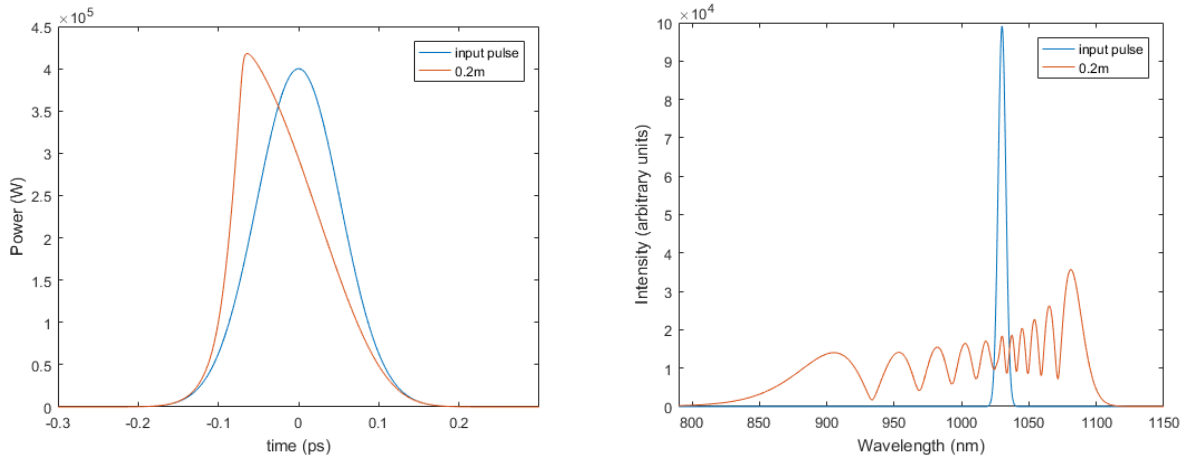


Fig 2.7: Time domain (left) and frequency domain simulations of self-steepening acting with SPM.

### 2.2.4 The Higher Order Nonlinear Schrodinger Equation

When equation 2.6 is corrected to include the higher order effects of third order dispersion, SRS, and self-steepening it take the following form [2],

$$\frac{\partial U}{\partial z} = -\frac{i\beta_2}{2}\frac{\partial^2 U}{\partial t^2} + \frac{\beta_3}{6}\frac{\partial^3 U}{\partial t^3} + i\gamma(|U|^2 U + \frac{i\lambda}{2\pi c}\frac{\partial |U|^2 U}{\partial t} - T_R U \frac{\partial |U|^2}{\partial t}) \tag{2.11}$$

where $T_R$ is a constant that approximates the Raman response of the fiber. This equation is known as the higher order nonlinear Schrodinger equation.

This equation has no simple analytic solution; however, section 3.1 will provide an outline of a simple, fast, and accurate numerical method for solving this equation.

# **Chapter 3:** Materials and Methods

The methods used in this type of investigation can often be quite complicated. This chapter will provide a brief overview of the experimental and numerical methods used, as well as some background information on how the optical fiber used in this investigation works.

## 3.1 The Split-Step Fourier Method

Since the higher order nonlinear Schrodinger equation presented in equation (2.11) does not have any simple analytic solutions it must be solved numerically in order to simulate the propagation of a pulse of light in optical fiber. A common numerical method used for solving the higher order nonlinear Schrodinger equation is known as the split-step Fourier method [2].

In order to understand this method first consider equation 2.11 rewritten in the following form.

$$\frac{\partial U}{\partial z} = (\widehat{D} + \widehat{N})U \tag{3.1}$$

Here $\widehat{D}$ is a differential operator which represents dispersive effects within the fiber given by

$$\widehat{D} = -\frac{i\beta_2}{2}\frac{\partial^2}{\partial t^2} + \frac{\beta_3}{6}\frac{\partial^3}{\partial t^3} \tag{3.2}$$

And $\widehat{N}$ is a nonlinear operator representing the nonlinear effects within the fiber given by

$$\widehat{N} = i\gamma(|U|^2 + \frac{i\lambda}{2\pi c}\frac{1}{U}\frac{\partial |U|^2 U}{\partial t} - T_R\frac{\partial |U|^2}{\partial t}) \tag{3.3}$$

In general, dispersive and nonlinear effects act together on a pulse as it propagates through fiber, however over a short distance dispersion and nonlinearity can be treated as independent of each other. Therefore, in order to determine how a pulse evolves over a short distance first consider

the effect of dispersion assuming no nonlinearity, and then consider the effect of nonlinearity assuming no dispersion. Integrating the differential equation in equation 3.1 over a small step size $h$ gives the following equation, which describes how the electric field envelope of an optical pulse changes over a short distance.

$$U(z+h,t) \approx U(z,t)\exp(h\widehat{D})\exp(\mathrm{h}\widehat{N}) \tag{3.4}$$

The nonlinear operator $\widehat{N}$ can be evaluated quite simply by plugging in values and computing the derivatives numerically, while the differential nature of $\widehat{D}$ means that it can not be evaluated directly and is typically evaluated in the Fourier domain. Hence the pulse evolution over a short distance is given by the following expression.

$$U(z+h,t) \approx FT^{-1}\left[\exp(h\widehat{D}(i\omega))FT\left(U(z,t)\right)\right]\exp\left(h\widehat{N}\right) \tag{3.5}$$

Where $FT$ is the Fourier transform operator, and $\widehat{D}(i\omega)$ is the dispersion operator converted to the Fourier domain by replacing all instances of $\frac{\partial}{\partial t}$ with $i\omega$, where $\omega$ is the Fourier domain frequency.

The expression given in equation 3.5 provides an approximation for the evolution of a pulse in optical fiber which can be evaluated quickly using the fast Fourier transform algorithm. This work utilizes a more accurate version of this method, known as the symmetrized split-step Fourier method. This method first evaluates the dispersive effects over a half step, then evaluates the nonlinear effects over a full step, and finally evaluates the dispersive term over another half step. This method has been shown to be more accurate than the non-symmetrized split-step Fourier method, with the symmetrized version having an error proportional to the cube of the step size whereas the non-symmetrized version has an error proportional to the square of the step size [2].

## 3.2 Photonic Crystal Fiber

The optical fibers used for this work are large mode area polarization-maintaining photonic-crystal fibers. Photonic crystal fibers are optical fibers which utilize the properties of photonic crystals (crystals which have a nanostructure that affects the motion of photons in a similar way to how an ionic lattice affects the motion of electrons in solids) in their design. The properties of these crystals enable the production of optical fibers with lower attenuation, larger mode areas, and higher damage thresholds than traditional glass fibers. There are a large variety of different fiber types that fall under the category of photonic-crystal fiber some examples of categories of photonic-crystal fiber include hollow core fiber, and photonic bandgap fiber. The fiber used in this work falls under a category known as hole-assisted fiber, which uses a solid core surrounded by a cladding containing a pattern of periodically spaced holes. These holes allow the cladding to have a very low refractive index, which allows the core to have an effective area up to ten times greater than what is possible in conventional fibers. Because fiber nonlinearity is inversely dependent on the fiber's mode area large mode area fibers have much lower nonlinearity than standard optical fibers.

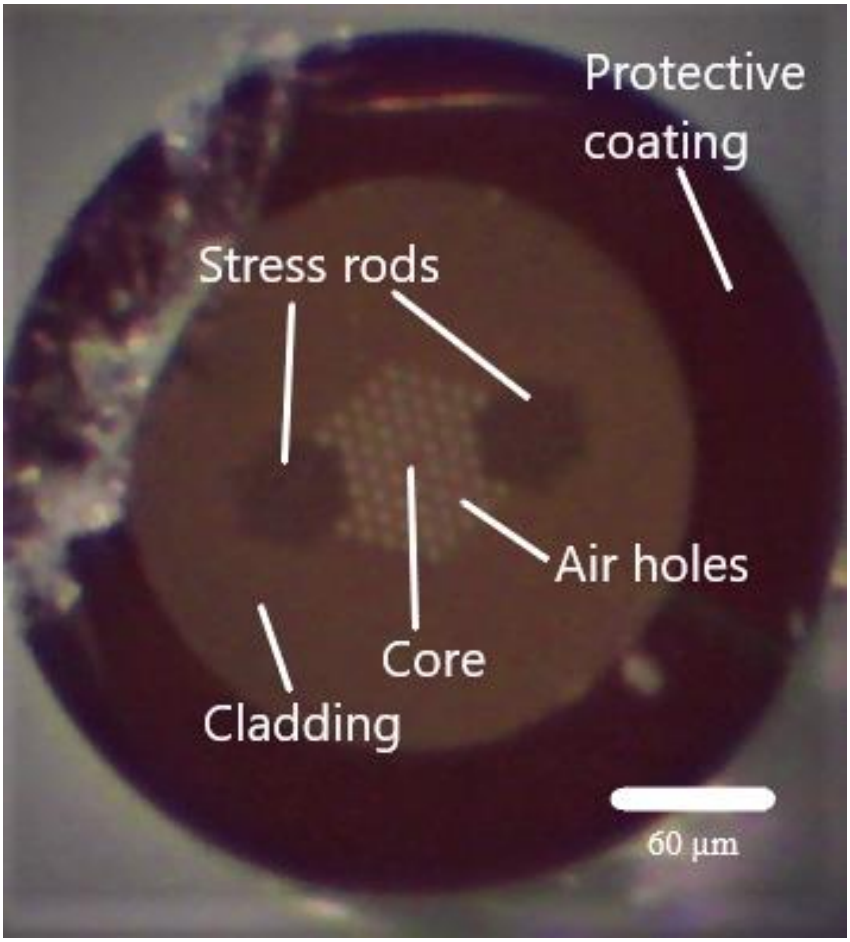


Fig 3.1: A brightfield microscope image of a fiber face with the various components labeled.

Figure 3.1 shows a microscope image of one of the fibers used in this work, with the air holes surrounding the core visible. On either side of the core there are two stress rods which run down the length of the fiber. These stress rods are used to induce strong birefringence within the fiber, because of this only light with polarization aligned with the stress rods is able to move through the fiber. This means that the input beam of light is able to propagate through the entire length of the fiber with no change to its polarization. This is useful for the application of spectral broadening to nonlinear optical microscopy since many forms of nonlinear optical microscopy require the laser source being used to have a well defined polarization.

# 3.3 Experimental Set Up

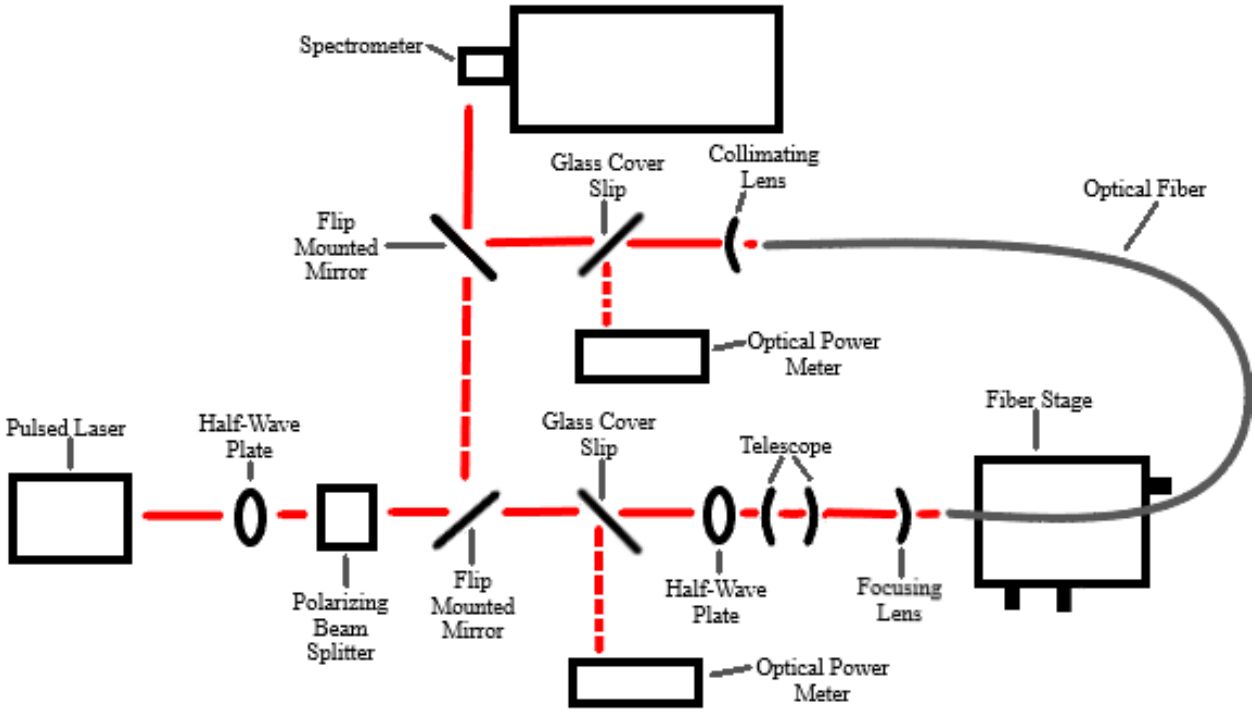


Fig 3.2: Diagram of the experimental set-up.

Fig 3.2 provides an overview of the major components of the experimental set up. A pulsed laser (Femtolux 3, EKSPLA) is directed through a half-wave plate and a polarizing beam splitter. This allows the beam power to be adjusted by rotating the half wave plate. A flip mounted mirror is then used to direct the beam towards either the fiber or the spectrometer. On the fiber beam path, a glass cover slip is used to reflect approximately 2% of the beam power onto an optical power meter which can then be calibrated to measure the power of the beam at the fiber. The main beam then goes through a half wave plate which rotates linearly polarized

light in order to obtain the correct polarization for polarization maintaining fibers. A telescope and focusing lens then focus the beam to the correct size and numerical aperture so that it can be coupled to the fiber.

The fiber is mounted to a three-axis fiber stage (Nanomax 300, Thorlabs) this stage allows the fiber to be positioned in three dimensions by adjusting three differential micrometers each having a resolution of 0.5 µm. A mirror mount (SC100-F3H, Newport) is attached to the fiber stage, the angle of the mirror mount can be adjusted in order to change the tilt angle of the fiber. By adjusting the fiber position and tilt angle the fiber can be placed such that its coupling efficiency is maximized (see section 3.2.2).

At the fiber output the beam is collimated by a lens and the output power is measured using another glass cover slip and power meter. The beam is then directed into the spectrometer (Wavescan NIR, APE) using a flip mounted mirror.

# 3.4 Fiber Preparation and Coupling

## 3.4.1 Measurement of Beam Diameter

In order to select the appropriate lenses to focus the laser beam into the fiber the laser beam diameter must first be measured. A simple and accurate method for doing this is known as the knife edge method. In this method the beam power is measured using an optical power meter. A razor blade is then inserted into the beam using a translation stage, and the position of the blade is measured at the points where the beam power drops to 90% and 10% of its original

value. This can then be used to calculate the $1/e^2$ diameter of the beam using the following formula [22].

$$d = 1.561(|x_{10} - x_{90}|) \tag{3.6}$$

Using this method, the $1/e^2$ beam diameter at the fiber was determined to be 3.17 ± 0.03 mm. This can now be used to determine what lenses are needed in order to couple the beam into the fiber.

## 3.4.2 Fiber Cleaving

To achieve good coupling efficiency the fiber must be cleaved properly, this ensures that the fiber face is uniform, and free from dust. Cleaving optical fiber by hand can be very difficult and often takes several attempts to ensure a proper cleave. It is important to note that photonic crystal fiber is often very expensive and cleaving it removes a small part (typically up to 2 cm), so great care should be taken during the cleaving process. The procedure used for cleaving optical fiber by hand is outlined below.

First the protective coating must be stripped from the end of the fiber using a fiber stripping tool. Next secure the end of the fiber to a surface using tape, leaving the position where the cleave will be made exposed. Now while keeping tension on the fiber gently drag a fiber scribe across the fiber, it is important that the right amount of pressure be used here as to much will cut through the fiber, and too little will result in the fiber not breaking cleanly in the next step. Next apply tension on the fiber back until it breaks, ensure that the fiber does not bend during this process as that could lead to an uneven break. The fiber face should be inspected using a microscope to ensure that the cleave is uniform and that there is no obvious damage. Here the fiber cladding should be free from scratches or debris, and the scribe mark should be no

larger than 5% of the cladding diameter. Fig 3.3 shows images of a fiber which has been properly cleaved, as well as one which has been poorly cleaved.

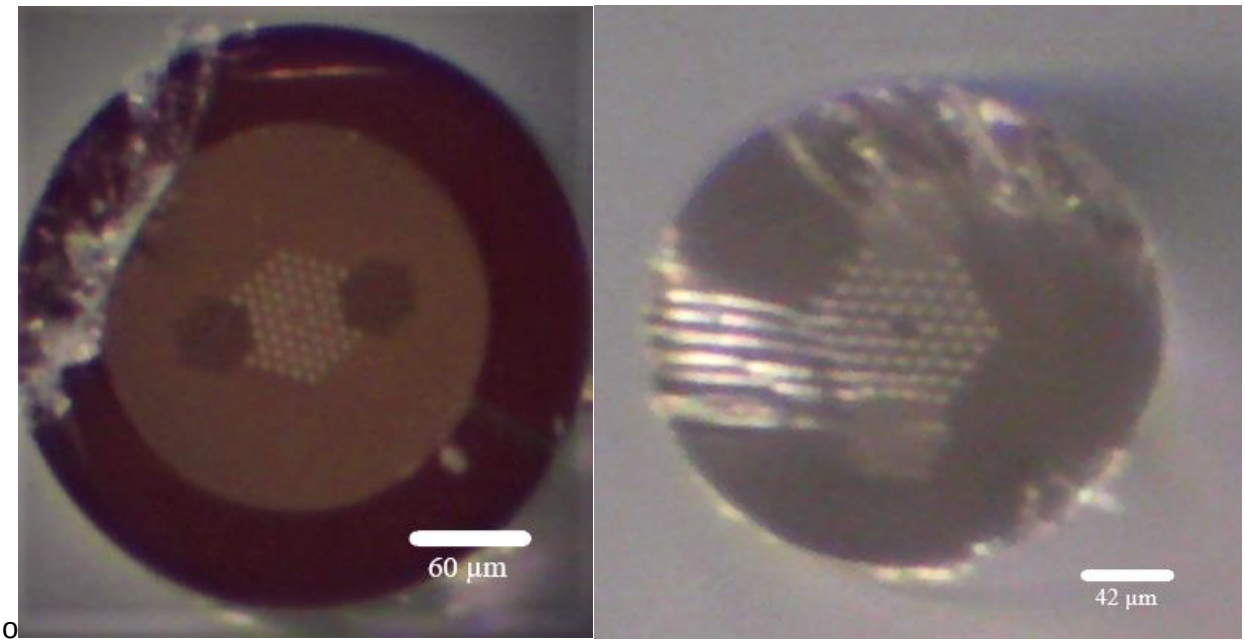


Fig 3.3: Brightfield microscope images showing a well cleaved fiber (left) and a poorly cleaved fiber (right). Note that the well cleaved fiber is free from damage on the face, and the scribe mark does not extend far onto the fiber face.

## 3.4.3 Fiber Coupling

To couple the beam to the fiber lenses must be used to focus the beam such that it meets two conditions. The beams width must be less than the mode field diameter of the fiber (the effective diameter of the fiber core), and the numerical aperture of the beam must be less than the numerical aperture of the fiber. If a focusing lens with focal length $f$ is used, then the minimum beam width ($w$) and numerical aperture ($NA$) are given by the following formulae [22].

$$w = \frac{4\lambda M^2 f}{\pi d} \qquad NA = d^2/\sqrt{d^2 + 4f^2} \tag{3.7}$$

Where $\lambda$ is the laser wavelength $d$ is the beam diameter and $M^2$ is the beam quality factor (assumed to be 1.2 for the Femtolux 3 laser). In order to achieve good coupling using commercially available lenses it may be necessary to use a telescope before the focusing lens to change the diameter of the input beam and get a more favourable minimum beam width. For the fiber used in this work (LMA-PM-15, NKT Photonics) the beam width must be smaller than 12.6 µm, and the numerical aperture of the beam must be less than 0.07. Here a lens with a focal length of 25 mm was used to achieve a minimum beam width of 11.4 µm and a numerical aperture of 0.06.

Once appropriate lenses have been selected to focus the beam into the fiber the fiber must be aligned to the beam. To do this first the fiber is mounted to a fiber stage, and the end of the fiber is placed near the focal point of the focusing lens. An optical power meter is then placed at the output end of the fiber. By adjusting the position of the fiber using the fiber stage the fiber is then raster scanned across the area near the focal point until an increase in power is detected by the power meter. Once a small amount of coupling is achieved the coupling efficiency can be maximized by making fine adjustments to the position and tilt angle of the fiber input end. Typical coupling efficiencies using this method are in the range of 50-75% however coupling efficiency can be severely affected by the quality of the fiber cleave, and by the goodness of the beam focusing.

# **Chapter 4:** Experimental Results

## 4.1 Effect of Pulse Energy on Spectral Broadening

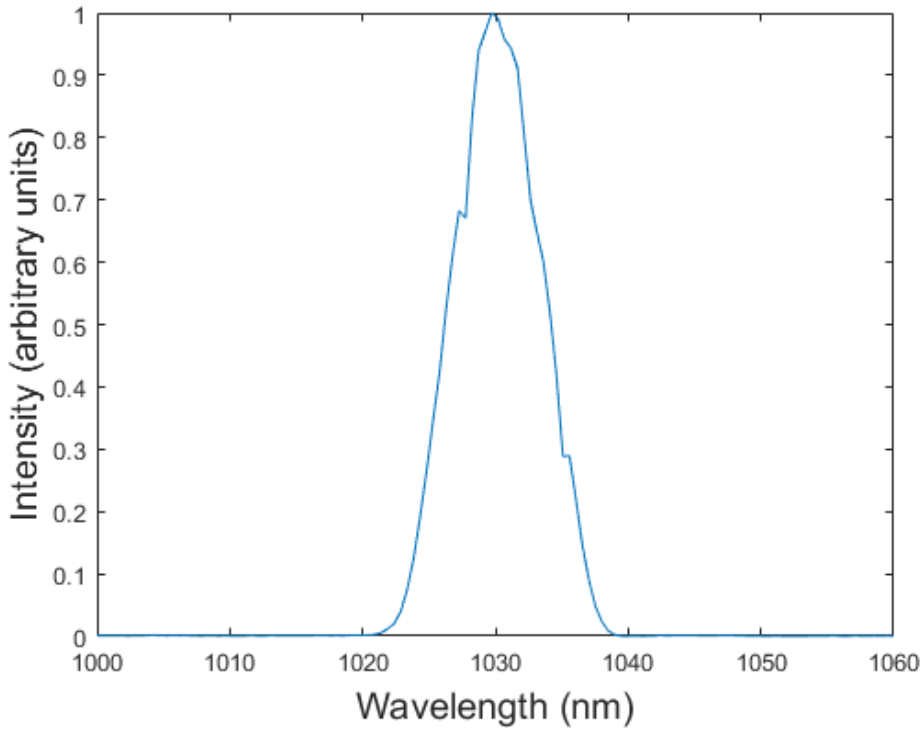


Fig 4.1: The spectrum of the laser that the fiber is coupled to, here the spectral width at full width half maximum is approximately 8 nm.

In order to understand how the spectrum of a 1030 nm laser with pulse duration between 245 and 5000 fs is affected by nonlinear and dispersive effects within optical fibers a first experiment will consider how changes in pulse energy, while keeping pulse duration and initial spectrum constant, effect the spectrum of the output pulse. In this experiment a 115 cm length of LMA-PM-15 photonic crystal fiber from NKT Photonics was free space coupled to a pulsed

laser source. Pulses of light with a center wavelength of 1030 nm (as shown in Fig 4.1) are propagated through the fiber at varying pulse energies, and the output spectrum of the pulses was recorded using a spectrometer. The pulse duration is held constant during this experiment.

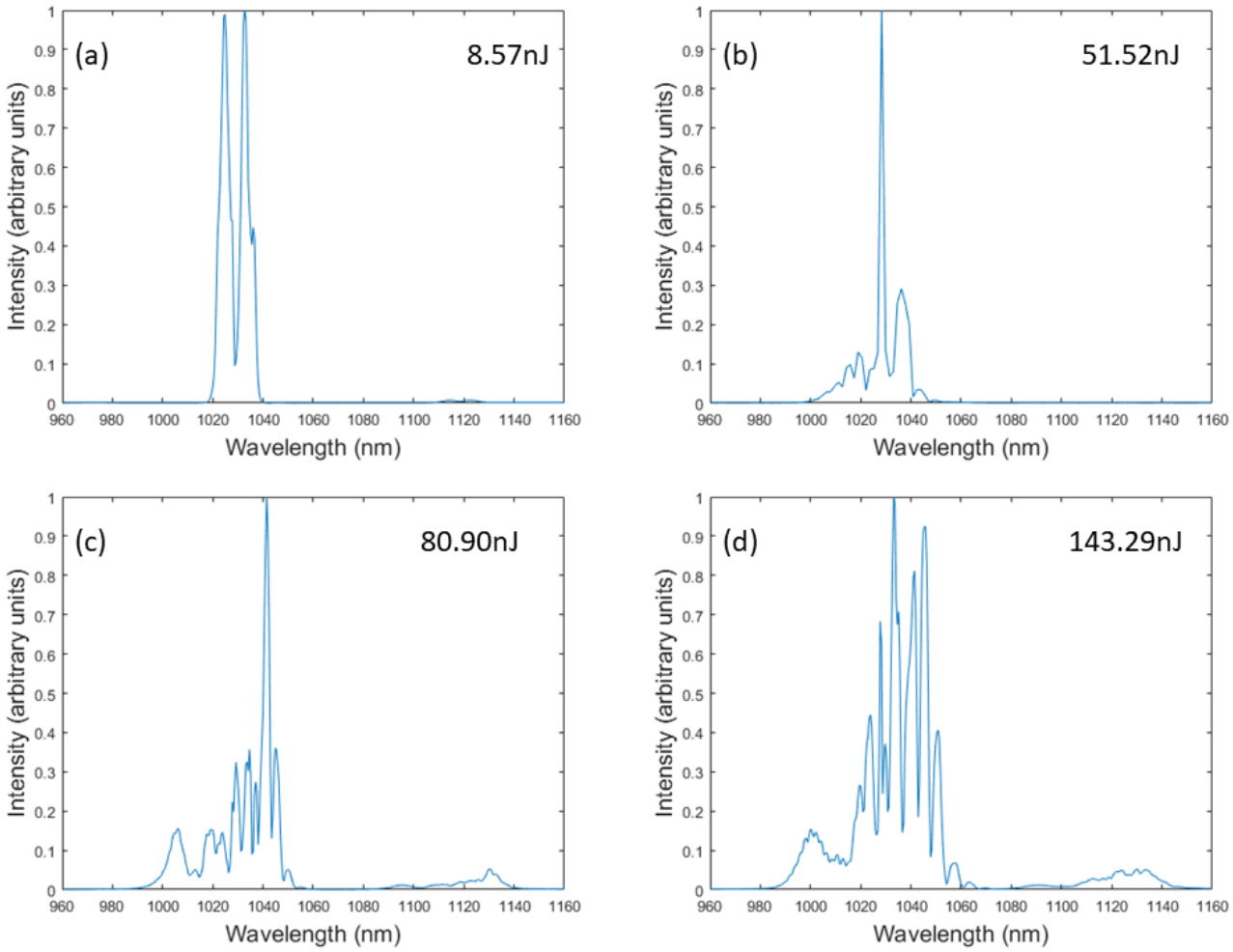


Fig 4.2: Normalized Output spectrum of 115 cm of LMA-PM-15 fiber at various pulse energies, the input pulse duration and spectrum were held constant during this experiment.

The normalized experimental spectra shown in Fig 4.2 show several interesting features. Fig 4.2 panel (a) shows that at lower pulse energies the spectrum breaks into two symmetric spectral lobes, which is characteristic of a pulse under the influence of pure SPM (see Fig 2.2). As the pulse energy is increased the large number of distinct peaks that is expected from SPM however at these higher energies the spectra take on a much more asymmetric shape as seen in Fig 4.2 panels (b)-(d). This asymmetric shape is likely due to several higher order optical effects such as self-steepening, and SRS starting to be the dominant effects on the pulse as the pulse energy is increased.

It is also important to note that while the output spectra are mostly concentrated into a series of connected peaks, in Fig 4.2 panels (c) and (d) there is a feature between 1120 and 1140 nm that is disconnected from the main spectrum. It is likely that this is a component of the pulse spectrum which has been redshifted due to SRS, however it is also possible that this feature is part of the input laser spectrum.

In order to get a quantitative idea of how spectral broadening is dependent on pulse energy the spectral width can be considered to be the distance between the leftmost and rightmost peak on the spectrum. The locations of the peaks can be approximately determined by using a Gaussian fit. Here features which are detached from the main spectrum, such as the peaks between 1120 and 1140 nm in Fig 4.2 panels (c) and (d), are not considered. The spectral widths determined using the technique are presented in table 4.1.

| Fig 4.2 Panel | Pulse Energy (nJ) | Leftmost Peak (± 1 nm) | Rightmost Peak (± 1 nm) | Center Values (±0.7 nm) | Spectral Width (± 1 nm) |
|---|---|---|---|---|---|
| (a) | 8.57 | 1025 | 1036 | 1030.5 | 11 |
| (b) | 51.52 | 1019 | 1037 | 1028.0 | 18 |
| (c) | 80.90 | 1005 | 1052 | 1028.5 | 47 |
| (d) | 143.29 | 1002 | 1063 | 1032.5 | 61 |

Table 4.1: Spectral widths of fiber output spectrum at various pulse energies.

The widths and center values presented in table 4.1 show that the spectral width of the output spectrum increases with pulse energy, and that this increase in spectral width is nearly symmetrical about the center wavelength of the input pulse. Assuming that this spectral broadening continues for higher pulse energies than this could be a possible method for wavelength tuning in microscopy applications where filters can be used to isolate different components of the spectrum. However, due to the symmetric nature of this broadening the spectral power density is greatly decreased compared to the input pulse, this will place some limitations on which wavelengths will be usable for practical applications.

## 4.2 Effect of Pulse Duration on Spectral Broadening

In addition to investigating the effect of varying pulse energy on spectral broadening the effect of changing pulse duration can also be investigated. In section 4.1 the effect of increasing the pulse energy of a nearly transform limited pulse with a duration of 245 fs was considered. Here

the effect of adding a chirp to the pulse such that it has a duration of 5 ps with no change to its initial spectrum will be considered using the same 115cm length of LMA-PM-15 fiber as was used in the previous section.

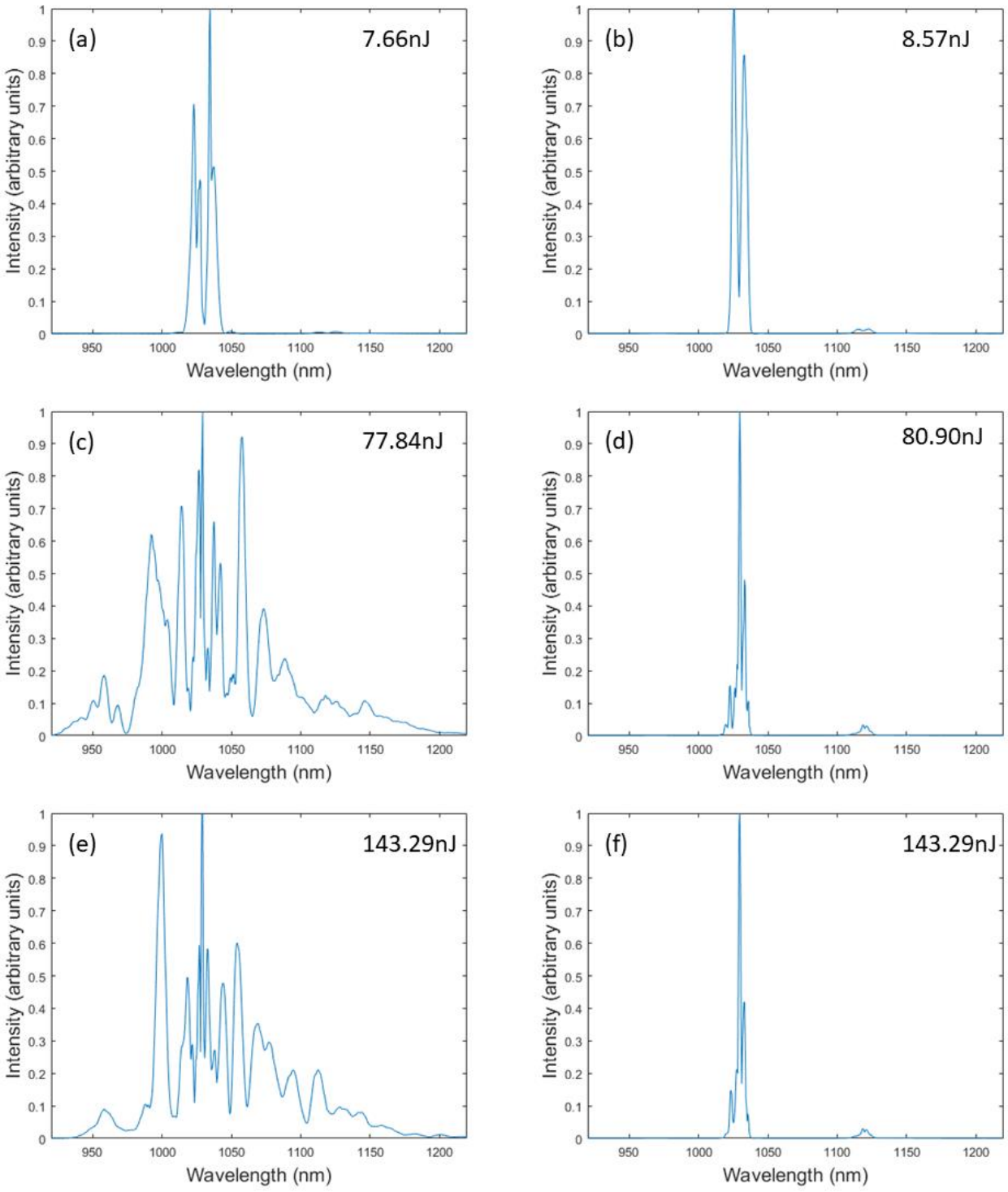


Fig 4.3: Fiber output spectra at different pulse energies (rows) for 245 fs near transform limited pulses (left) and 5 ps chirped pulses (right).

Since the 5 ps pulse used in this experiment is not transform limited and has the same spectral width as the nearly transform limited 245 fs pulse it is expected that the higher order optical effects discussed in chapter 2 will still have a noticeable effect on the pulse. As an example of this the three spectra for 5 ps pulses (Fig 4.3 panels (b), (d), (f)) still show asymmetric broadening and not the symmetric spectral broadening characteristic of SPM. However, there are some key differences between the spectra for the 245 fs and 5 ps durations. For example, the 245 fs spectra (Fig 4.3 panels (a),(c), (e)) become much broader as the pulse energy is increased, while the 5 ps spectra become deformed but only undergo a very small amount of spectral broadening.

Table 4.2 presents data for spectral broadening for each pulse energy and duration, the spectral width is defined as the distance between the leftmost and rightmost peaks on the spectrum, as in section 4.1. This data shows that the spectral broadening for the 245 fs pulses is much greater than that for the 5 ps pulses with the 245 fs pulses being broadened to over 150 nm whereas the 5 ps pulses do not exceed 10 nm of spectral width. This is likely because although the spectra in Fig 4.3 were measured for three sets of similar pulse energies the increase in pulse duration leads to a decrease in the peak power of the pulse, with the peak power at 245fs being more than 20 times that at 5 ps with equal pulse energy. This means that adjusting the pulse duration could be an effective method of modulating the amount spectral broadening generated, which will be useful in wavelength tunning for microscopy applications.

| Fig 4.3 Panel | Pulse Duration (fs) | Pulse Energy (nJ) | Spectral Width (±1 nm) |
|---|---|---|---|
| (a) | 245 | 7.66 | 15 |
| (b) | 5000 | 8.57 | 7 |
| (c) | 245 | 77.84 | 193 |
| (d) | 5000 | 80.90 | 10 |
| (e) | 245 | 143.29 | 165 |
| (f) | 5000 | 143.29 | 10 |

Table 4.2: Comparison of spectral widths for pulses of similar pulse energy and different pulse durations.

## 4.3 Effect of Fiber Length on Spectral Broadening

Another parameter which can be considered when investigating how nonlinear effects in optical fiber effect the spectrum of a pulse of light is the length of optical fiber used. In this experiment otherwise identical LMA-PM-15 fibers with length of 40 cm and 115 cm were used and near transform limited 245 fs pulses with a center wavelength of 1030 nm were propagated through the fibers at various pulse energies. The output spectrum from the fiber was then measured using a spectrometer.

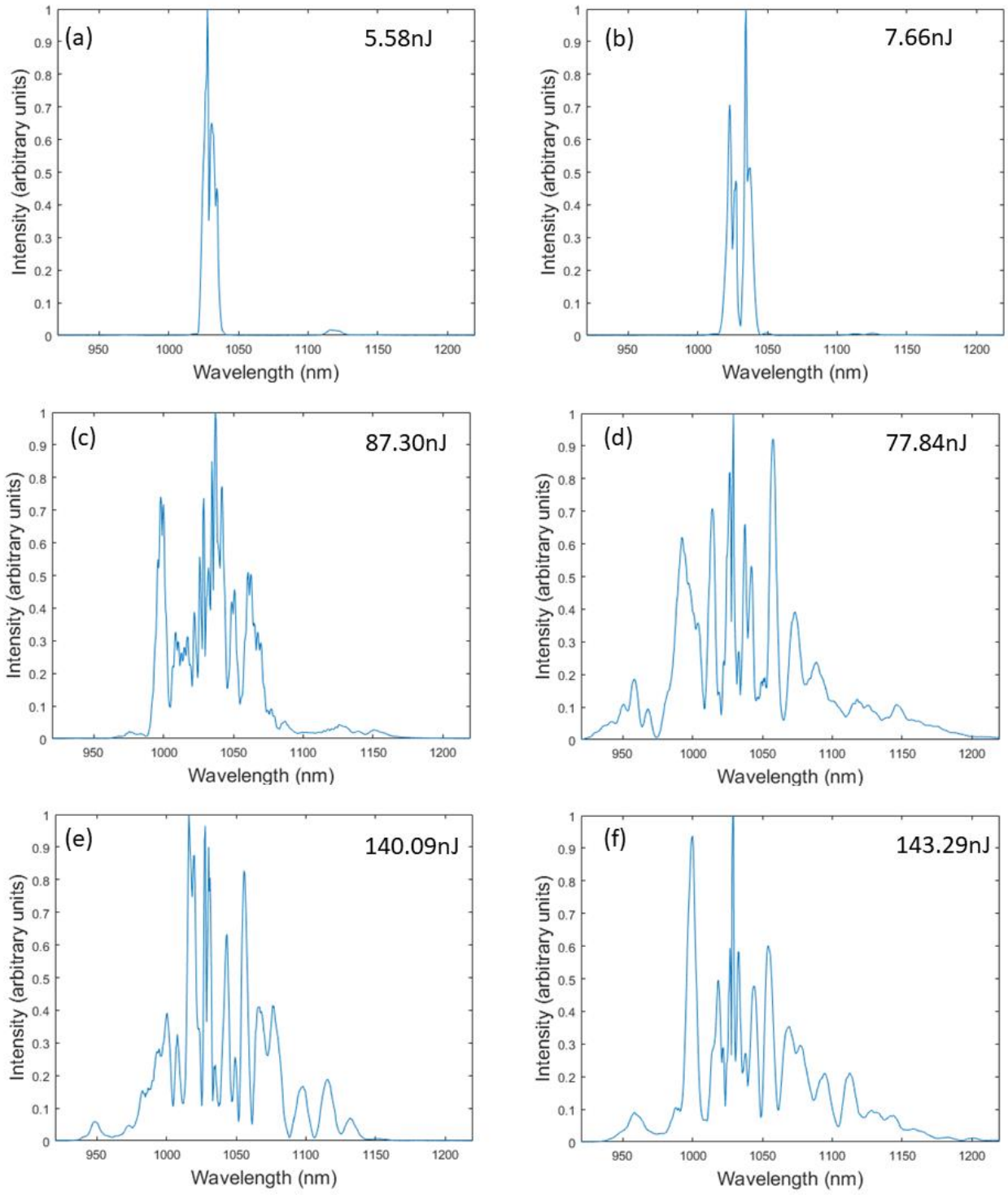


Fig 4.4: Output spectra for the 40cm fiber (left) and the 115cm fiber (right) at various pulse energies.

The results shown in Fig 4.4 provide some very interesting insight into how spectral broadening occurs within optical fibers. Table 4.3 provides the resulting spectral width for each fiber length and pulse energy. In this experiment the long fiber was nearly three times longer than the shorter fiber, and for the lower pulse energies in Fig 4.4 panels (a) and (b) the spectral width is approximately three times greater for the longer fiber. However, at the higher pulse energies shown in panels (c), (d), (e) and (f), there is a much smaller difference between spectral widths between the longer and the shorter fiber for similar pulse energies. It is particularly interesting that for panels (e) and (f) the resulting spectral width from the short fiber seems greater than that from the long fiber. From Fig 4.4 panels (e) and (f) it can be seen that this is in fact a result of the convention used for measuring spectral width. Spectrum e for the short fiber has peaks further from the center of the spectrum, however panel (f) has peaks closer to the center of the spectrum with more of a smoothly decreasing region on either side. This suggests that the added fiber length has an effect of 'smoothing' the spectrum, giving long continuous regions, rather than the rapidly oscillating structures that are seen near the center of each spectrum. This indicates that for applications where a broad and relatively uniform spectrum is desired, such as supercontinuum generation, a longer fiber might be desirable.

It is also interesting to note that the relatively small differences in spectral width between panels (c), (d) and panels (e), (f) indicates that the majority of the spectral broadening occurs within some initial short section of fiber. This is possibly a result of the overall spectral power density being reduced as the spectrum broadens. This is a useful result since it suggests that similar spectral widths could be obtained using only a few centimeters of fiber, this means that a

shorter fiber could be used in the future which would reduce the amount of power lost as a result of attenuation and bending losses within the fiber.

| Fig 4.4 Panel | Fiber Length (cm) | Pulse Energy (nJ) | Spectral Width (nm) |
|---|---|---|---|
| (a) | 40 | 5.58 | 5 ± 2 |
| (b) | 115 | 7.66 | 15 ± 1 |
| (c) | 40 | 87.30 | 165 ± 1 |
| (d) | 115 | 77.84 | 193 ± 3 |
| (e) | 40 | 140.09 | 182 ± 4 |
| (f) | 115 | 143.29 | 165 ± 4 |

Table 4.3: Comparisons of spectral widths of pulses with similar energy using fibers of different two different lengths.

# **Chapter 5:** Numerical Simulations

In chapter 4 experimental data showing how nonlinear effects alter the spectrum of a pulse of light was considered. In this chapter numerical simulations using the method outlined in chapter 3.1 will be considered. Before any simulations can be carried out values must be selected for the various constants present in the higher order nonlinear Schrodinger equation (eq 2.13).

To start with these simulations will use an initial center wavelength of 1030 nm. A common core material for optical fibers is fused silica (this is the core material of the fibers used in chapter 4) at 1030 nm fused silica has a nonlinear refractive index of $n_2 = 2.19 \cdot 10^{-20} m^2 W^{-1}$ [23], and a GVD constant of $\beta_2 = 1.897 \cdot 10^{-26} s^2 m^{-1}$ [24]. Values for the third order dispersion parameter and the Raman constant are generally less well defined than the other constants however the typical order of magnitude of these constants is generally known. For third order dispersion typically $\beta_3 \approx 10^{-40} s^3 m^{-1}$ [2]. The Raman constant has been measured by various authors and has been found to be within the range of 3-6 fs, in this chapter a value of $T_R$ = 3 fs will be used [25]. All simulations in this section use a step size of 0.1 mm results with this step size were found to be nearly identical to results with smaller step sizes.

## 5.1 Impact of Higher Order Effects on Spectral Broadening

In chapter 2 the assertion was made that higher order optical effects such as self-steepening, third order dispersion, and SRS need only be considered for optical pulses with durations less than a few picoseconds. In this sections that assertion will be tested using numerical simulations. Here the propagation of transform limited optical pulses with various durations will be simulated once with all optical effects included, and once with only the effects

of SPM and GVD included. These simulations will use a fiber mode field diameter of 12.6 μm and a length of 30 cm. The simulated pulses have a Gaussian temporal profile and a constant peak power of 100 kW (this corresponds to a pulse energy of 25 nJ at 250 fs).

The simulation results presented in Fig 5.1 and Fig 5.2 clearly show that the higher order effects of third-order dispersion, self-steepening, and SRS can be ignored for pulse durations of more than a few picoseconds. There are very obvious visual differences between the simulated spectra for 250fs, 500fs, and 1ps, as shown in panels (a) – (f) and the higher order terms are clearly needed to ensure accurate simulations at these pulse durations. However, for the spectra at 5 and 10 ps as shown in Fig 5.2 panels (g) – (j) the differences between the spectra are more subtle. In order to characterize the differences between these spectra the magnitudes and positions of the left most and right most peaks can be considered.

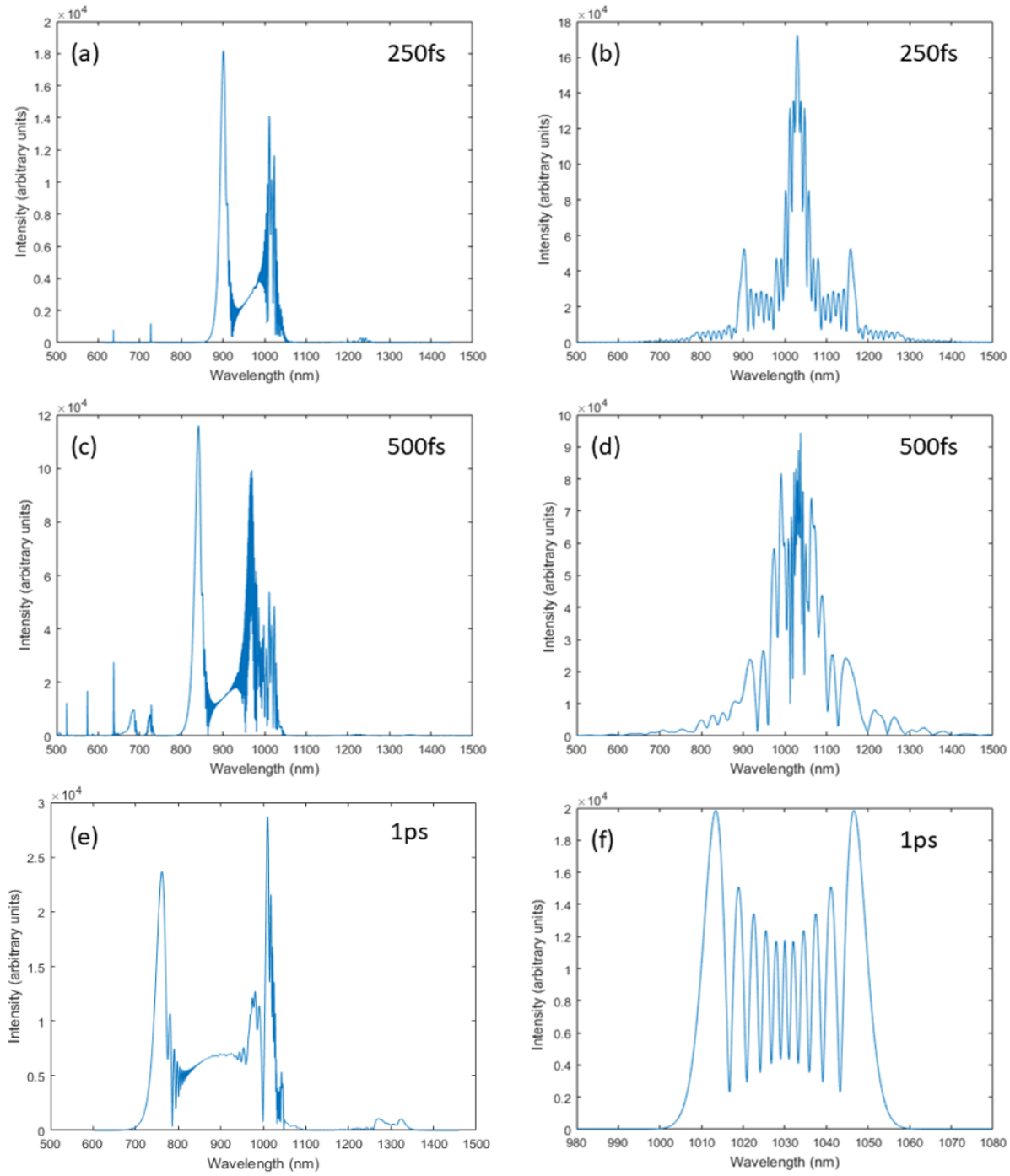


Fig 5.1: Simulated spectra with GVD, SPM, third-order dispersion, SRS, and self-steepening (left) and simulated spectra with GVD and SPM (right).

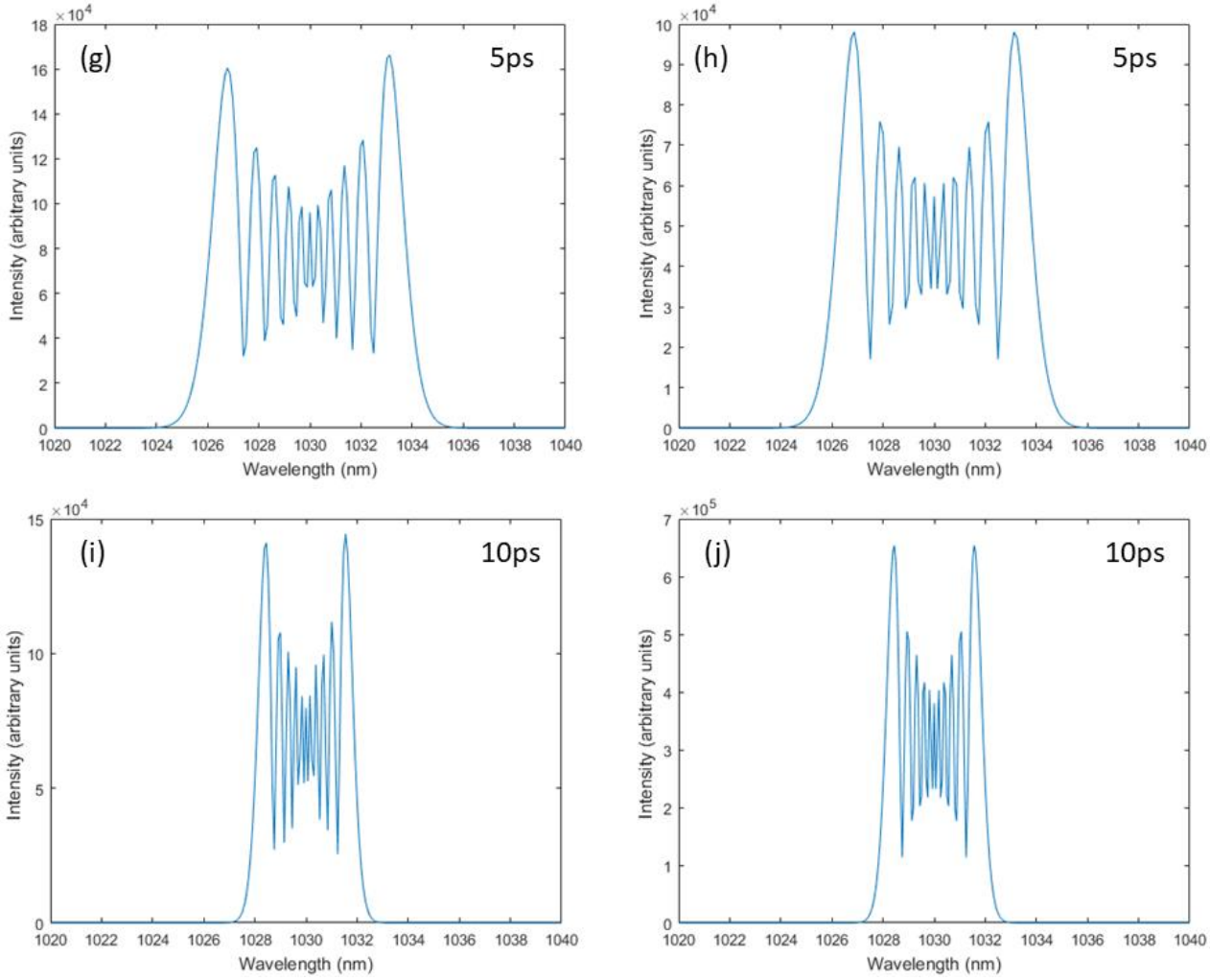


Fig 5.2: Simulated spectra with GVD, SPM, third-order dispersion, SRS, and self-steepening (left) and simulated spectra with GVD and SPM (right).

For the 5 ps spectra (Fig 5.2 panels (g) and (h)) there is a difference of less than 0.01% between the wavelengths of the two maxima, and for the lower order spectrum there is a difference of approximately 0.0001% between the magnitude of the two peaks. For the higher order 5 ps spectrum (panel (h)) there is a difference of approximately 3.6% between the

magnitudes of the two peaks. There is a similarly small difference for the 10 ps spectra in panels (i) and (j).

From these numbers it is clear that there is little difference in the amount of spectral broadening between the two sets of spectra. However, there is an asymmetry between the peaks on the higher order spectra which is not present on the lower order spectra. This asymmetry is likely due to the effect of self-steepening which is known to cause asymmetry in SPM broadened spectra. As was discussed in section 2.2.3 self-steepening arises due to large differences between the center and the wings of the temporal profile of a pulse. Since in these simulations peak power and not pulse energy was held constant there is still quite a large difference between the peak and the wings of the pulse in the 10 ps case.

It is interesting to note that the simulated spectra in Fig 5.1 panels (a), (c), and (e) all show very large blue shifted peaks. Similar blue shifted peaks can be seen in the experimental data presented in Fig 4.3 panel (e), and Fig 4.4 panels (c) and (f). However, the flat structure seen in these simulations between the blue shifted peak and the main peak is not present in any of the experimental spectra presented in chapter 4.

## 5.2 Effect of Pulse Shape on Spectral Broadening

Depending on how a pulsed laser is constructed there are a variety of different pulse shapes which are possible. Most common are lasers whose pulse power profiles are best described by either a Gaussian or a $sech^2$ pulse shape (the power profiles of each of these pulse shapes can be seen in Fig 5.3). Here numerical simulations will be used to determine if the slight

differences between these pulse shapes leads to any change in the output spectrum from the fiber. This is of interest since the fundamental soliton has a $sech^2$ temporal profile (see section 2.1.3) hence any difference between the output spectra for these two pulse shapes could cause problems for applications involving optical solitons such as soliton self-frequency shift.

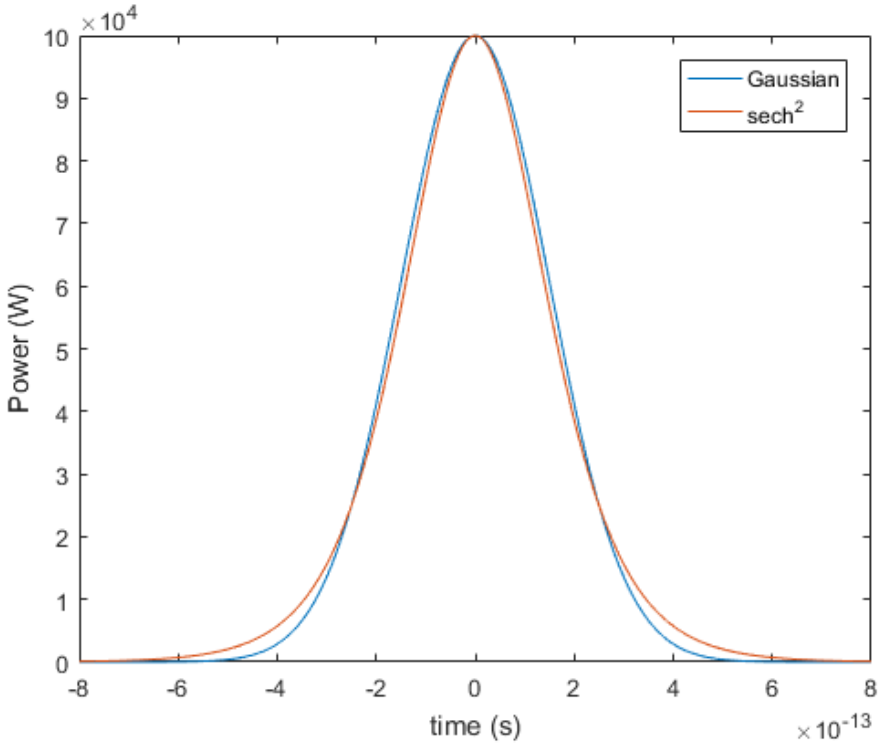


Fig 5.3: The power profiles of Gaussian and $sech^2$ pulse shapes, both pulses have a peak power of 100 kW and a FWHM duration of 500 fs.

Here 500 fs pulses with both Gaussian and $sech^2$ will be simulated at various pulse energies over 30 cm of simulated optical fiber with a mode field diameter of 12.6 µm.

From the simulations presented in Fig 5.4 it is clear that there are minor qualitative differences in the structure of the output spectra between the Gaussian input pulses in panels (a), (c), (e) and the $sech^2$ input pulses in panels (b), (d), (f). One very notable feature of these spectra

is the peak in panels (c), (d), (e), (f) which is located between 1200 and 1400 nm and is disconnected from the main spectrum. As was discussed in section 2.2.2 these disconnected redshifted peaks are likely the result of SRS within the fiber. It is interesting that the redshifted peaks in panels (d), (e), (f) resemble the redshifted peaks that are expected as a result of soliton self-frequency shift, however, the main spectrum has clearly been greatly broadened, and not maintained its original shape as is expected from a soliton (nor does it show the symmetric broadening expected from a higher order soliton).

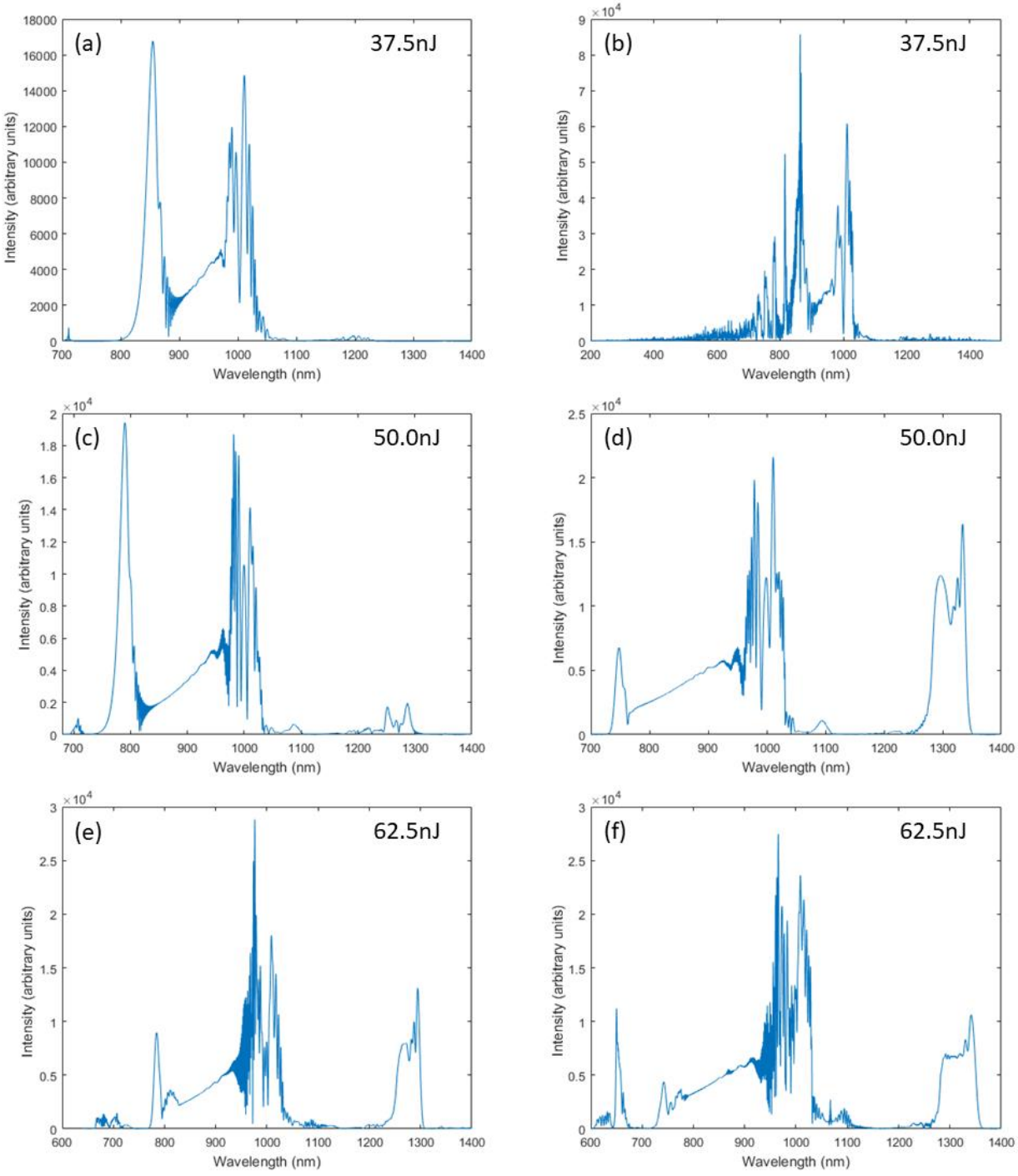


Fig 5.4: Simulated output spectra for Gaussian input pulse (left) and $sech^2$ input pulse (right) at various pulse energies.

A likely explanation for this is that over some short initial section of the fiber the pulse is able to propagate relatively undisturbed, it is likely during this stage when the majority of the red shifting occurs. Eventually the effects of third order dispersion and self-steepening will cause the shape of the pulse to change significantly, this is what causes the broad central region of the spectra shown in Fig 5.4. This idea is supported by the simulations shown in Fig 5.5, in which the time domain behaviour of the pulse is seen to be somewhat stable over the first few centimeters (Fig 5.5 (a)), but after that the pulse becomes unstable and is rapidly broken up by higher order effects.

One question which remains here is why in Fig 5.4 is the redshifted peak very prominent in panel (d) whereas in panel (c) the redshifted peak is far less prominent. A likely reason for this is that Gaussian shaped pulses are less stable than $sech^2$ shaped pulses. This explanation makes sense since, as was discussed in section 2.1.3, soliton solutions to the nonlinear Schrodinger equation have a $sech^2$ shaped temporal profile. Because of this it is likely that a Gaussian shaped pulse will break up over a shorter length of fiber than a $sech^2$ shaped pulse meaning that the Gaussian pulse will be less influenced by SRS during this stable phase resulting in a smaller redshifted peak.

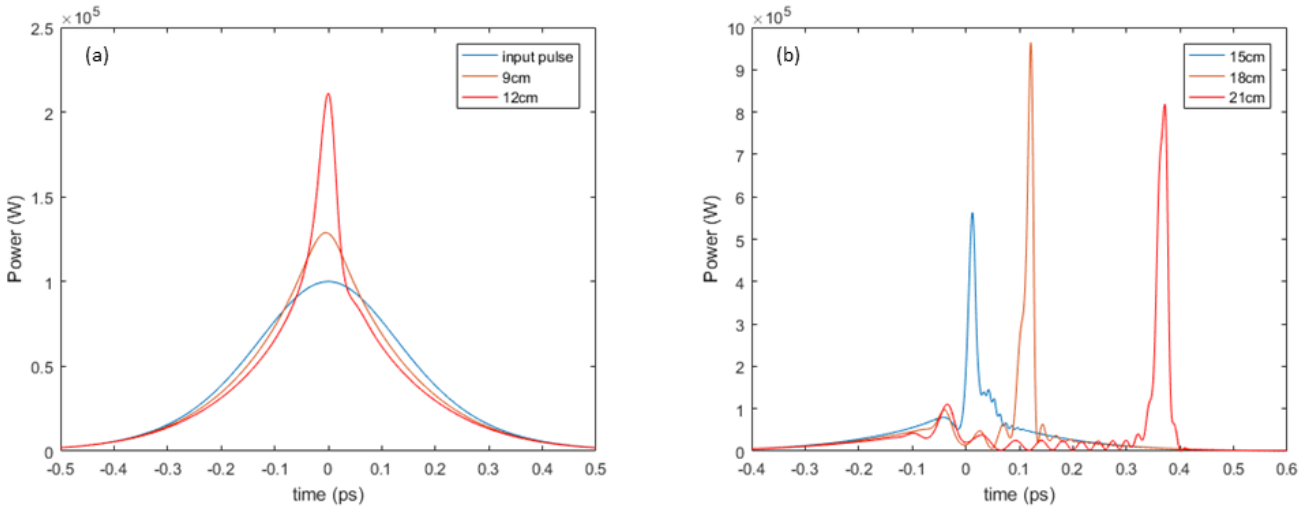


Fig 5.5: Simulations showing the time domain evolution of a 500 fs $sech^2$ shaped optical pulse through several lengths of optical fiber.

# **Chapter 6:** Conclusions and Future Work

## 6.1 Conclusions

This investigation has provided some very interesting insights on how various factors influence the spectral broadening brought about by nonlinear optical effects in photonic crystal fiber. This includes results from both experimental work, and numerical simulations.

The experimental work done here has yielded a number of interesting results. This includes the result that higher pulse energies lead to a greater amount of spectral broadening, that increasing pulse duration, while keeping pulse energy and initial spectrum constant, leads to a decrease in the amount of spectral broadening in optical fiber. An experiment comparing the output spectra from fibers of different lengths showed that using a longer fiber does not necessarily increase the width of the output spectrum implying that the majority of the spectra broadening occurs within some short initial section of the fiber. It was also found that longer fibers have the effect of 'smoothing' the output spectrum, which indicates that longer fiber might be more useful for applications such as supercontinuum generation. It is interesting to note that the experimental spectra presented in chapter 4 do not closely match any of the methods of spectral broadening discussed in section 1.2, with most of the experimental spectra resembling a halfway point between pure SPM and supercontinuum generation.

The results of the experimental work done here were augmented through the use of numerical simulations. The results of these simulations have shown that higher order effects, such as third-order dispersion, self-steepening, and SRS, have greatly reduced effects on transform limited optical pulses with durations greater than 5 ps. This confirms that these higher

order effects only become dominant on a pulse whose duration is on the order of picoseconds or less. Simulations were also used to show that small differences in the temporal profile of the input pulse can lead to significant differences in the output spectra. Simulations of the temporal behaviour of optical pulses was used to show that these eventually become unstable. This behaviour is a possible explanation for why redshifted peaks, characteristic of SRS, appear in some spectra but not in others.

Overall, the work done here has provided some valuable insights into how optical fibers can be used to broaden the spectra of ultrashort optical pulses. These insights will be very useful going forwards in applying this spectral broadening to construct a wavelength tunable laser source for nonlinear optical microscopy.

## 6.2 Future Work

This investigation has left various areas open for future work. The maximum pulse energy used in chapter 4 was unfortunately limited by technical problems to a maximum of approximately 220 nJ once these technical problems are resolved pulse energies of over 2000 nJ will be possible. This is expected to lead to much more spectral broadening than was recorded in chapter 4, which is extremely advantageous for microscopy applications.

Other varieties of optical fiber might also be evaluated for their applications in wavelength tunning for optical microscopy applications. This might include fibers of larger or smaller mode areas, and fibers with different core materials including hollow core fibers. The effectiveness of these fibers can be evaluated initially using numerical simulations in order to determine the possible value of using these fibers.

Finally, the fiber output can be coupled to a microscope and used to tune the laser wavelength for the investigation of various samples. This is expected to give more information on the structure of the sample under investigation then is possible using a single wavelength.

## 6.3 Acknowledgments

I would like to thank my supervisor Dr. Richard Cisek for his help in guiding me in this project over the past year. I would also like to thank Dr. Danielle Tokarz whose prior experience with optical fiber was very helpful in constructing the experimental setup used in this investigation. I also thank my family and friends for their support as I have worked on this project. Finally, I acknowledge the support of the Natural Science and Engineering Research Council of Canada Discovery Grants Program (RGPIN-2018-05444), the Canada Foundation for Innovation John R. Evans Leaders Fund, Canada's Research Support Fund and Saint Mary's University.

# Bibliography

[1] J.Hecht, *City of light — the story of fibre optics*. 2004.

[2] G. P. AGRAWAL, *Nonlinear fiber optics*, 3rd ed. 1989.

[3] R. H. Stolen, "Phase-Matched-Stimulated Four-Photon Mixing in Silica-Fiber Waveguides," *IEEE J. Quantum Electron.*, 1975, doi: 10.1109/JQE.1975.1068571.

[4] E. P. Ippen and R. H. Stolen, "Stimulated Brillouin scattering in optical fibers," *Appl. Phys. Lett.*, 1972, doi: 10.1063/1.1654249.

[5] R. H. Stolen and E. P. Ippen, "Raman gain in glass optical waveguides," *Appl. Phys. Lett.*, 1973, doi: 10.1063/1.1654637.

[6] R. H. Stolen and C. Lin, "Self-phase-modulation in silica optical fibers," *Phys. Rev. A*, 1978, doi: 10.1103/PhysRevA.17.1448.

[7] D. Tokarz *et al.*, "Characterization of pancreatic cancer tissue using multiphoton excitation fluorescence and polarization-sensitive harmonic generation microscopy," *Front. Oncol.*, 2019, doi: 10.3389/fonc.2019.00272.

[8] P. Campagnola, "Second harmonic generation imaging microscopy: Applications to diseases diagnostics," *Anal. Chem.*, 2011, doi: 10.1021/ac1032325.

[9] G. C. Valley, "Photonic analog-to-digital converters," *Opt. Express*, 2007, doi: 10.1364/oe.15.001955.

[10] D. Dahan and G. Eisenstein, "Tunable all optical delay via slow and fast light propagation in a Raman assisted fiber optical parametric amplifier: a route to all optical buffering," *Opt. Express*, 2005, doi: 10.1364/opex.13.006234.

[11] W. Liu, C. Li, Z. Zhang, F. X. Kärtner, and G. Chang, "Self-phase modulation enabled,

wavelength-tunable ultrafast fiber laser sources: an energy scalable approach," *Opt. Express*, 2016, doi: 10.1364/oe.24.015328.

[12] W. Liu, S.-H. Chia, H.-Y. Chung, R. Greinert, F. X. Kärtner, and G. Chang, "Energetic ultrafast fiber laser sources tunable in 1030–1215 nm for deep tissue multi-photon microscopy," *Opt. Express*, 2017, doi: 10.1364/oe.25.006822.

[13] M. L. Ferhat, L. Cherbi, and I. Haddouche, "Supercontinuum generation in silica photonic crystal fiber at 1.3 μm and 1.65 μm wavelengths for optical coherence tomography," *Optik (Stuttg).*, 2018, doi: 10.1016/j.ijleo.2017.09.111.

[14] Y. Shen *et al.*, "Picosecond supercontinuum generation in large mode area photonic crystal fibers for coherent anti-Stokes Raman scattering microspectroscopy," *Sci. Rep.*, 2018, doi: 10.1038/s41598-018-27811-5.

[15] J. P. Gordon, "Theory of the soliton self-frequency shift," *Opt. Lett.*, vol. 11, no. 10, p. 662, 1986, doi: 10.1364/ol.11.000662.

[16] D. Tokarz *et al.*, "Intravital imaging of osteocytes in mouse calvaria using third harmonic generation microscopy," *PLoS One*, vol. 12, no. 10, pp. 1–15, 2017, doi: 10.1371/journal.pone.0186846.

[17] B. Li, M. Wang, K. Charan, M. Li, and C. Xu, "Investigation of the long wavelength limit of soliton self-frequency shift in a silica fiber," *Opt. Express*, vol. 26, no. 15, p. 19637, 2018, doi: 10.1364/oe.26.019637.

[18] J. H. Lee, J. Van Howe, C. Xu, and X. Liu, "Soliton self-frequency shift: Experimental demonstrations and applications," *IEEE J. Sel. Top. Quantum Electron.*, vol. 14, no. 3, pp. 713–723, 2008, doi: 10.1109/JSTQE.2008.915526.

[19] R. W. Boyd, Ed., "Nonlinear Optics", Third Edit., Burlington: Academic Press, 2008.

[20] J. H. Jing Huang and J. Y. Jianquan Yao, “Estimation of the fourth-order dispersion coefficient \beta4,” *Chinese Opt. Lett.*, 2012, doi: 10.3788/col201210.101903.

[21] F. DeMartini, C. H. Townes, T. K. Gustafson, and P. L. Kelley, “Self-steepening of light pulses,” *Phys. Rev.*, 1967, doi: 10.1103/PhysRev.164.312.

[22] K. Purvis, R. Cisek, and D. Tokarz, “New Activity for Instrumental Analysis: Laser Beam Profiling,” *J. Chem. Educ.*, 2019, doi: 10.1021/acs.jchemed.9b00484.

[23] P. Kabaciński, T. M. Kardaś, Y. Stepanenko, and C. Radzewicz, “Nonlinear refractive index measurement by SPM-induced phase regression,” *Opt. Express*, 2019, doi: 10.1364/oe.27.011018.

[24] I. H. Malitson, “Interspecimen Comparison of the Refractive Index of Fused Silica*,†,” *J. Opt. Soc. Am.*, 1965, doi: 10.1364/josa.55.001205.

[25] A. K. Atieh, P. Myslinski, J. Chrostowski, and P. Galko, “Measuring the Raman Time Constant (TR) for Soliton Pulses in Standard Single-Mode Fiber,” *J. Light. Technol.*, 1999, doi: 10.1109/50.744227.